STUDY OF DYNAMIC RESPONSE OF DOUBLY FED INDUCTION GENERATOR DURING GRID INTERCONNECTION & FAULT CONDITION

Dissertation submitted in partial fulfillment of the requirements for the award of degree of

Master of Engineering
in
Power System and Electric Drives

Submitted By:
Ajay Kushwaha
(Regn. No. 801141002)

Under the supervision of:
Inderpreet Singh
Lecturer, EIED

July 2013

ELECTRICAL AND INSTRUMENTATION ENGINEERING DEPARTMENT
THAPAR UNIVERSITY,
(Established under section 3 of UGC act, 1956)
Patiala, 147004
Punjab, India

CERTIFICATE

I hereby certify that the work which is being presented in this dissertation entitled "STUDY OF DYNAMIC RESPONSE OF DOUBLY FED INDUCTION GENERATOR DURING GRID INTERCONNECTION & FAULT CONDITION" in partial fulfilment of the requirement for the award of degree of Master of Engineering in Power Systems and Electric Drives submitted in Electrical and Instrumentation Engineering Department of Thapar University, Patiala, is an authentic record of my own work carried out under the supervision of Mr. Inderpreet Singh, Lecturer, EIED.

The matter presented in this dissertation has not been submitted for the award of any other degree of this or any other university.

Ajay Kushwala 15/07/13

(Ajay Kushwaha)

It is certified that the above statement made by the student is correct to the best of our knowledge and belief.

15/7/13

Inderpreet Singh

Lecturer, EIED

Thapar University, Patiala

S. Ghosh

Dr. Smarajit Ghosh

Head of Department, EIED

Thapar University

Patiala

Dr. S.K. Mohapatra

Dean of Academic Affairs

Thapar University

Patiala

ACKNOWLEDGEMENT

I would like to express my gratitude to my supervisor Mr. Inderpreet Singh for his continued support during the period of my study and research and for his valuable advices that contributed in success of this thesis.

I am very thankful to Dr. Smarajit Ghosh, Professor & Head of Department, EIED & Mrs. Manbir Kaur, Associate Professor & P.G. Coordinator, EIED along with entire faculty and staff members of Electrical and Instrumentation Engineering Department for their sincerity and efforts in their work.

I would also like to thank my parents for their encouragement to me for studying here and their patience on parting me for the whole study duration.
I would also like to thank all the loyal friends that their virtues can never be forgotten.
Finally, I would like to extend my gratitude to all those persons that their advices directly or indirectly helped me in this process and contributed in success of this work.

Ajay Kushwaha
15/07/13
Ajay Kushwaha

ABSTRACT

Modern technology in the wind turbines has increased the penetration of wind power generation up to considerable level in the power system grid. This leads to more complex, sophisticated and reliable interconnection requirements for reliable power system operation. According to the requirements, the wind farm operation shall not affect the grid dynamic behavior and operation e.g. starting up, cut off, wind speed variations etc, but in actual scenario when grid is attributed to fault and voltage dips, the disconnection of the wind farm creates shedding of loads results in unreliable power supply. This occurs mostly in the case of 3 phase faults in transmission network. For this reason depending on the voltage level of the connection point, network operators require wind farms to have Fault Ride Through (FRT) capabilities and so to withstand specified voltage dips. There are more areas of problems and constraint such as grid capacity constraints, power quality issues, protection issues and ancillary services issues. In order to mitigate above mentioned problems, the study and analysis of wind turbines in power system are required. For performing these studies there is need of steady state and dynamic models of various configurations of wind turbine. Due to various advantages variable speed wind turbines are preferred to fixed speed wind turbines. Among variable speed wind turbines doubly fed induction generator (DFIG) based wind turbines are more popular because of their inherent capabilities. In the present study a dynamic model of DFIG based WECS has been developed and various studies have been performed in PSCAD/EMTDC.

LIST OF CONTENTS

LIST OF TABLES

LIST OF FIGURES

LIST OF ABBREVATIONS

ABBREVATIONS	CLARIFICATION
FSWT	Fixed Speed Wind Turbine
GSC	Grid Side Converter
LVRT	Low Voltage Ride Through
MPP	Maximum Power Point
MPPT	Maximum Power Point Tracking
PLL	Phase Locked Loop
RSC	Rotor Side Converter
SCIG	Squirrel Cage Induction Generator
SFO	Stator Flux Oriented
VC	Vector Control
VOC	Voltage Oriented Control
VSWT	Variable Speed Wind Turbine
WECS	Wind Energy Conversion System
WRIM	Wound Rotor Induction Machine
WT	Wind Turbine

LIST OF NOMENCLATURES

SYMBOL	DISCRIPTION
P_{air}	Power in air flow,
P	Air density (Kg/ m^3)
A	Area swept by blade. (m^2)
ν	Velocity of wind. (m/s)
C_P	Power Coefficient
$P_{\text{wind turbine}}$	Power of wind turbine
λ	Tip speed ratio
ω	Rotational speed of rotor. (rad/sec)
R	Blade length (m)
P_M	Mechanical power of the turbine
λ_{opt}	Optimal tip speed ratio
ω_M	Mechanical speed of the turbine
T_M	Turbine mechanical torque
P_m	Mechanical power
ω_s	Synchronous speed
ω_r	Rotor speed
P_r	Rotor power
P_g	Power delivered to the grid
V_s	Stator Voltage
V_{ds}	d-axis stator voltage
V_{qs}	q-axis stator voltage
I_s	Stator current
I_{ds}	d-axis stator current
I_{qs}	q-axis stator current
λ_s	Stator linkage flux
λ_{ds}	d-axis stator linkage flux
λ_{qs}	q-axis stator linkage flux
V_r	Rotor side voltage
V_{dr}	d-axis rotor side voltage

V_{qr}	q-axis rotor side voltage
I_r	Rotor side current
I_{dr} .	d-axis rotor side current
I_{qr}	q- axis rotor side current
λ_r	Rotor linkage flux
λ_{dr}	d-axis rotor linkage flux
λ_{qr}	q-axis rotor linkage flux
r_s	Stator resistance
r_r	Rotor resistance
L_s	Stator inductance
L_m	Magnetizing inductance
L_r	Rotor inductance
L_{ls}	Stator side leakage inductance
L_{lr}	Rotor side leakage inductance
σ	Leakage coefficient
P_s	Stator active power
Q_s	Stator reactive power
P_r	Rotor active power
Q_r	Rotor reactive power
Q_{total}	Total reactive power
T_e	Electromagnetic torque
P	Number of poles
J	Inertia
C	Dc link capacitance
E_c	Energy of dc link capacitor
P	power across capacitor
V_{DC}	Dc link capacitor voltage
i_d	d- axis current
i_q	q-axis current
I_{ms}	Stator magnetizing current
V^*_{dr}	d-axis reference rotor voltage
V^*_{qr}	q-axis reference rotor voltage
R_r	Rotor resistance

ω_{slip}	Slip speed
Q_g*	Reference reactive power
I_{dr}*	d-axis reference rotor current
$\omega_{ref\_}$	Reference rotor current
Ira_ref	Reference rotor current of phase a
Irb_ref	Reference rotor current of phase b
Irc_ref	Reference rotor current of phase c
ϕ_s	Location of rotating flux vector
ϕ_r	Location of rotor angle
ϕ_{slip}	Slip angle
θg	Grid angle
i_{1d}	d- axis grid side current
i_{1q}	q- axis grid side current
i_{1a}	Grid side current of phase a
i_{1b}	Grid side current of phase b
i_{1c}	Grid side current of phase c
V_g	Grid side voltage
i_{qref}*	*q*-axis current reference
E_{cap}	dc voltage of capacitor
E_{capref}*	Reference dc voltage of capacitor
V_{ai1}	Fundamental component of a- phase voltage
m_a	Modulation index
L_g	Grid side inductance
V_{dref1}	d-axis reference voltage
V_{qref1}	q-axis reference voltage
i_{dg}*	d- axis grid side reference current
i_{qg}*	q- axis grid side reference current
Ir	Rotor current

Chapter-1

INTRODUCTION

1.1 OVERVIEW

Due to environmental concerns caused by excessive exploitation of conventional resources, now the focus is diverted to non-renewable resources especially solar & wind as these are environmentally clean and eco-friendly. In the beginning, wind power generation was negligible as compared to conventional plants due to lack of sophisticated wind turbine (WT) technology but now with the development of new technologies; there has been an exponential growth in the wind power.

The total installation of wind power capacity reaches around 282.4 GW around the world and it is increased by 44.7 GW within year 2012 i.e. (18.8%).

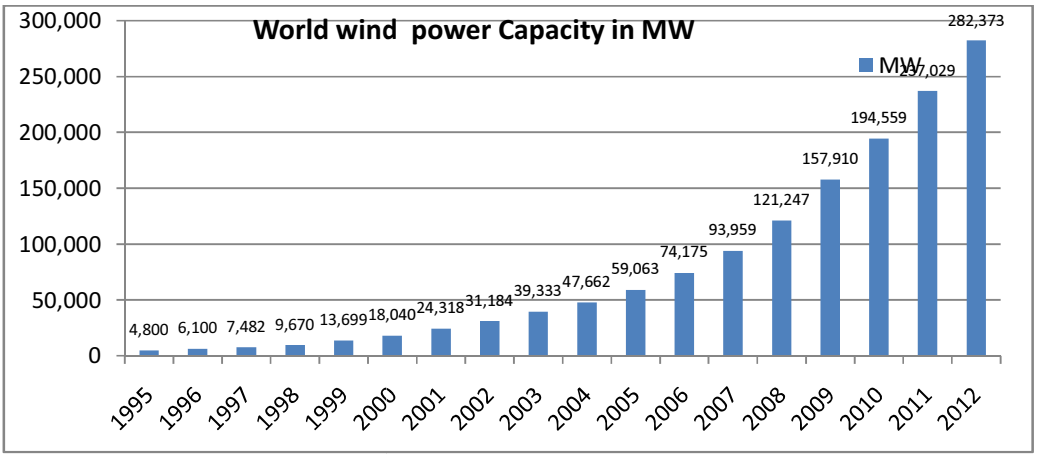

Fig. 1.1 (Growth of Wind power installation around the world)

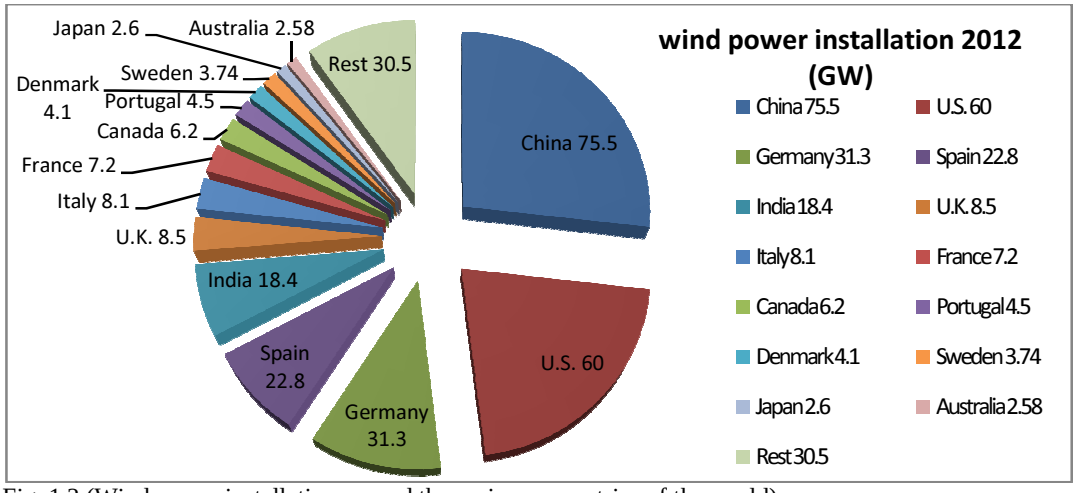

Fig. 1.2 (Wind power installation around the various counntries of the world)

Global wind industry growth has been driven mainly by China (75,564 MW), the US (60,007MW), Germany (31,307MW), Spain (22,796 MW) and India (18,421MW) [1]. India has grown its installation up to 18,421 MW at the end of year 2012 (16.1 % increment in 2012). The total wind farms are grown to 443 in India.

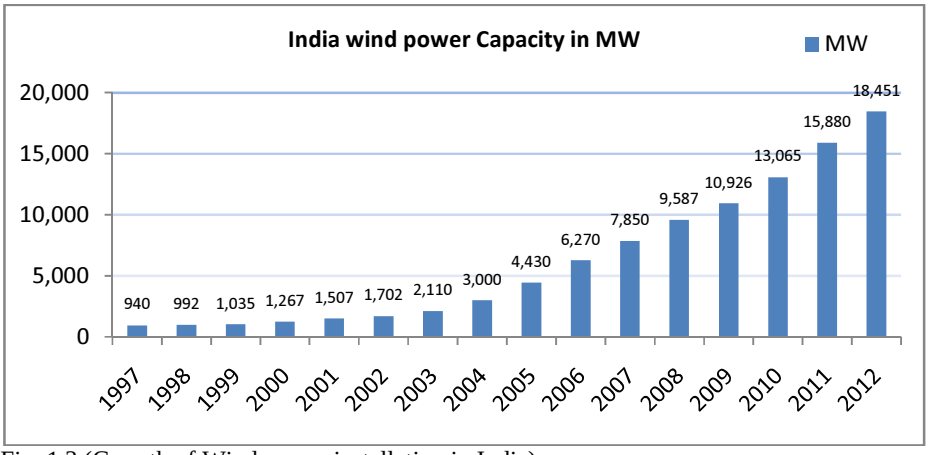

Fig. 1.3 (Growth of Wind power installation in India)

The major companies leading in global market are Vestas Wind Systems, GE wind energy, Gamesa, Enercon, suzlon, Siemens, Acciona, Gold wind, Nordex and Sinovel. The wind power installation includes some of project in India, which is undertaken by above mentioned companies.

1.3 **LITERATURE SURVEY**

With increasing penetration of wind-derived power in interconnected power systems, it has become necessary to model the complete wind energy systems in order to study their impact and also to study wind plant control [2]. Wind energy generation equipment is most often installed in remote, rural areas. These remote areas usually have weak grids, often with voltage unbalances and under/overvoltage conditions [3-4]. The traditional wind turbine generator systems employ squirrel-cage induction generators (SCIGs) to generate wind power. The fixed speed system is more simple and reliable [5]. The major problems observed with Fixed Speed Wind Turbine (FSWT) based SCIG are voltage fluctuation (flicker) & Low voltage ride through (LVRT), when connected to weak power grids where the wind power penetration levels are high [6]. It has one more disadvantage of requiring capacitors at the stator terminals to provide for the reactive power demand of the machine [7].

Grid connected FSWT based SCIG WTs often produce active power with significant fluctuations due to wind speed variations, the wind gradient and the tower shadow effect [8]. When connected to a weak power grid and during a grid fault, the over-speeding of the WTs can cause voltage instability [9]. As a result, utilities typically disconnect the WTs immediately from the grid when such a contingency occurs. With the rapid increase in penetration of wind power in power grids, tripping of many WTs in a large wind farm during grid faults may begin to influence the overall power system stability [6].

The FSWTs have no speed control capability and cannot provide voltage or frequency support when connected to the power grid [6]. For wind energy applications, various induction generator schemes have been proposed. The variable speed, constant voltage-constant frequency self-excited induction generator for autonomous systems has largely been discussed [7**].** For variable-speed wind generation using the doubly fed induction generator (DFIG), the rated speed settings, gearbox ratios, and machine and converter ratings were described [10].

Compared to the fixed-speed SCIG WTs, the DFIG WTs can provide decoupled active and reactive power control of the generator, more efficient energy production, improved power quality and improved dynamic performance [11, 12]. SCIG severely limits the energy output of a WT. In case of variable speed systems, comparison shows that using a wound rotor induction machine (WRIM) of similar rating can significantly enhance energy capture [5]. It is possible to transfer maximum power to the network in a wide range of wind speeds without exceeding the ratings of the induction generator [7]. The wind energy conversion system (WECS) using a grid-connected fully-controlled double-output induction generator is considered and the conditions of transferring maximum power to the grid are investigated [7].

The concept of a variable speed wind turbine (VSWT) driving a DFIG has received increasing attention because of its noticeable advantages over other Wind Turbine Generating systems [5, 9, 12, 13, 14, 15]. DFIG-based WT are more popular on account of their favourable cost/performance attribute resulting primarily from the need for a much smaller converter rating compared to the machine rating [11]. The cost of power converter can be reduced greatly by employing doubly fed configuration such as a wound rotor machine as compared to full capacity configuration [12, 16].

DFIGs are widely used in modern WTs due to their power control capability; variable speed operation, low converter cost, and reduced power loss as compared to other solutions such as fixed speed induction generators or fully rated converter systems [15]. The converter design and control technique using an ac/dc/ac converter in the rotor circuit of Doubly Fed Induction Machine (Schrebius drive) is explained. It was a standard drive option for high power applications involving a limited speed range. The power converters only need to handle the rotor side power [17].

A vector control (VC) strategy can be used for decoupled control of active and reactive power drawn from the supply was proposed [18]. The VC technique used for the independent control of torque and excitation current are explained [19]. A model of the induction generator written in appropriate d-q reference frame to facilitate investigation of control strategies. Also reference frame models have been developed for doubly fed induction machines [20-21]. The power circuits, control system required for a rectifier are fully explained, along with the strategy employed to achieve closed loop regulation of d.c. link voltage, a sinusoidal current waveform, full four quadrant power flow to the supply and the desired power factor [18]. A detailed design of the DFIG using back-to-back PWM voltage source converters in the rotor circuit, they also validated the system experimentally considering a grid connected system [22]. DFIGs and a four-quadrant ac-to-ac converter connected to the rotor windings increases the transient stability margin of the electrical grids, when compared with the case where the fixed speed wind systems with cage generators are used [13].

In speed control mode operation, the aero-turbine can be operated at a constant speed by blade-pitch control of the WT even under varying wind speeds. This is possible since rotor circuit is capable of bidirectional power flow [2]. The doubly fed induction machine can be operated in generating mode in both sub-synchronous and super-synchronous modes [23]. The SCIG controlled over a range of sub-synchronous and super-synchronous speeds, using the novel secondary EMF signal generator, shows considerable advantage over sub-synchronous systems based on the Kramer technique [24] and does not have the stability problems normally associated with doubly fed machines [10]. The steady-state analysis of a wound-rotor induction generator operated at varying shaft speeds in the sub-synchronous and super-synchronous regions, by control of both the magnitude and direction of slip power is studied [25].

Energy extraction from a DFIG WT depends not only on the induction generator but also on the control strategies developed using different orientation frames. Various types of control designs have been proposed for studying the behavior of DFIG based wind-turbine system during normal and fault AC grid conditions [12, 22, 14, 26, 27, 28]. Different orientation frames and controller structures for the grid side converter (GSC) are analyzed. In [29], the generation of active power during unbalanced conditions is investigated. The same approach could be used in order to guarantee reactive power production during outages [30].

The control of the reactive power flow in DFIG drive allows production of reactive power independently of the active power and with both inverters. The active power output is normally determined by wind conditions. For the determination of reactive power capability for a given active power output, a number of system boundaries have to be considered. Also, the reactive power capability is subject to several limitations resulting from the voltage, current, and speed, which change with the operating point [11].

An optimum control strategy, which maximizes the total electrical power output of the DFIG is determined, the limitations of naturally commutated convertor circuits and their effects on the output power characteristic of the system are also discussed [25]. In [31] a state feedback regulator for active and reactive power in DFIG drives was proposed and compared to a proportional–integral controller by simulation. In addition to an exhaustive literature research, active and reactive power integral controllers with nested voltage and phase angle control loops, as well as sensitivity and stability analysis for a single distributed generation unit, are provided in [32]. Decoupled control of the electromagnetic torque and the reactive power using a sensor less scheme for the DFIG was proposed in [33]. Case studies on active and reactive power flow in wind farms were carried out in [34] using induction generators and in [35] using the DFIG. The recorded results pointed out the superior dynamics of the latter topology.

The DFIG is controlled using VC [12, 19, 36], which decouples the rotor currents into active power (or torque) and reactive power (or flux) components and adjusts them separately in a reference frame fixed to either the stator flux or voltage. Current controllers are then utilized to regulate the rotor currents [15]. DFIGs are controlled using VC based on rotor current decoupling, which are either stator flux oriented (SFO) [19, 22] or stator voltage oriented / voltage oriented control (VOC) [12].

Most existing models widely use VC based on SFO. However, the existing control designs assume the stator voltage is ideal, i.e., the frequency and amplitude of the stator or grid voltage are constant and the dynamic characteristic of the stator magnetizing current is not considered [22, 27, 28] Such a system can provide good dynamic response during normal operation condition but the performance may be degraded during AC voltage disturbance. Pena gave a detailed design of the DFIG using back-to-back PWM voltage source converters in the rotor circuit and they also validated the system experimentally considering a grid connected system [22]. The *dq* VC, stator-voltage-oriented can be called "grid flux oriented" control [46]. In this scheme, the *d*-axis is aligned with the stator-voltage space vector (instantaneously) The DFIG usually operates in VC mode based on the PI controllers in a synchronous reference frame either to the SFO or stator voltage oriented (or VOC) frames. The DFIG with PI controllers and its performance under normal operation conditions has been discussed in a number of publications [37, 36, 38, 15, 39] It is well known that the DFIG performance with PI controllers is excellent in normal grid conditions, allowing independent control of the grid active and reactive power [30, 40].

In [2, 32], the SFO frame is used to develop the DFIG wind power extraction mechanisms. Another approach, for example, direct power control strategies for DFIG WTs using the SFO frame [41], has also been proposed recently while VOC frame is normally not used for DFIG design. System based on VOC has also been used to control DFIG system [12, 42]. In [12], VOC was proposed for controlling DFIG system under normal operation, but no detailed design of decoupling circuit was given and a constant stator voltage was assumed. In [42], VOC control was used to investigate the fault current of DFIG. However, as no decoupling circuits were used, so that control response was inadequate during transient condition.

The method only utilizes the estimated stator flux so as to remove the difficulties associated with rotor flux estimation**.** The method selects appropriate voltage vectors based on the stator flux position and active and reactive power errors. Thus, the difficulties associated with the rotor flux estimation are removed [43]. There is special approach to improve DFIG stability under unbalanced conditions using the VOC frame [44, 45]. In [44] an analysis and control design of a DFIG based wind generation system operating under unbalanced network conditions is studied , a DFIG system model in the positive and negative synchronous reference frames is presented to enhance the stability of the DFIG under unbalanced voltage supply. In [45], it is shown that a DFIG control strategy can enhance the standard speed and

reactive power control with controllers that can compensate for the problems caused by an unbalanced grid by balancing the stator currents and eliminating torque and reactive power pulsations. Doubly fed machines, naturally, have a pair of poorly damped poles near the grid frequency. Fast inner current loops have a fast response time, but also tend to push the poorly damped system poles toward the right half plane [46]. when the stator phase voltages supplied by the grid are unbalanced, the torque produced by the induction generator is not constant. Instead, the torque has periodic pulsations at twice the grid frequency, which can result in acoustic noise at low levels and at high levels can damage the rotor shaft, gearbox, or blade assembly [47].

DFIG-based WTs can be well understood [12, 48, 22, 49]. DFIG systems are conventionally controlled using stator VOC [12], [48] or SFO [22], [49] controls based on d-q decoupling. In [50], a rotor position phase locked loop (PLL) is used which acquires the rotor position and rotor speed simultaneously for the implementation of the decoupled P-Q control in the DFIG. The rotor position PLL is designed to operate without the knowledge of any parameter of the DFIG except the magnetization reactance.

In [51], comparison between SFO and VOC reference frames is done and it is shown that the performance of DFIG wind power extraction is similar to using both VOC and SFO frames. But, it is found that a conventional wind power extraction approach using the SFO frame could deteriorate the power quality of the DFIG system while it is more stable to estimate the position of the stator-flux space vector by simply adding -90 degree to the stator-voltage space vector. This paper investigates and compares wind power extraction from a DFIG WT using stator voltage and stator oriented frames. This paper analysis how wind power extraction control of DFIG WT is converted to speed control and then how speed and reactive power control of WT is converted to generator current control using the two different orientation frames.

For protection survey, it is possible for WTs using DFIG to stay connected to the grid during grid faults by crowbar protection. The key of the technique is to limit the high currents and to provide a bypass for it in the rotor circuit via a set of resistors that are connected to the rotor windings without disconnecting the converter from the rotor or from the grid [14].

For the survey for other control schemes, the direct to power scheme decouples DFIG rotor current into two parts representing active and reactive power separately. The control of machine active and reactive power is achieved by adjusting these two rotor currents using PI

controllers. One main drawback for Direct Power Control scheme is that system performance highly depends on accurate machine parameters such as stator, rotor resistances and inductance. Thus performance degrades when actual machine parameters depart from values used in the control system due to saturation, temperature variation etc [41].

The main drawback for SFO-VC is its linear nature which does not consider the discrete operation of power electronics converter [15]. Thus, in order to maintain system stability over the whole operation range and adequate dynamic response under both normal and abnormal conditions, the current controller and its control parameters must be carefully tuned [36]. This effectively reduces the VC's control bandwidth and robustness during changing operation conditions.

1.4 OBJECTIVES OF THE PRESENT WORK

The objective of the dissertation is to study the dynamic behaviour/response of DFIG configuration with the implementation of control schemes on back-to-back converters. This study aims to tune the control techniques (i.e. SFO and VOC) successfully along with the use of Industrial controllers. (i.e. PI controllers) The objective is to achieve stable response of DFIG when subjected to grid integration, fault, and wind speed variation respectively. The overall theme is to achieve robustness of DFIG configuration. Also for that hardware protection (crowbar) is studied and incorporated in model.

1.5 ORGANISATION OF DISSERTATION

This dissertation has been organized in six chapters. In chapter ,1 basic introduction of wind energy generation, its modern scenario, literature review and glimpse of dissetation is incorporated. In chapter 2, basic theory of wind energy system is explained. It includes classification, characteristics and control system along with grid integration issues/requirements. In chapter 3 basic overview of DFIG configuration, operating modes along with dynamic modeling is explained. Further in chapter 4 the model of DFIG connected to grid is developed. The implementation of control scheme, protection etc. in model is explained. In chapter 5 the simulation results and explanation/verifications are incorporated. At last in chapter 6 conclusion of work and future scope are discussed.

CHAPTER 2
WIND: A SOURCE OF ELECTRICAL ENERGY

2.1 CONSTRUCTIONAL ASPECTS

The wind energy systems consist of several parts to achieve kinetic energy to electric energy conversion. The wind kinetic energy is converted to mechanical energy by the blades mounted on the rotor hub. The rotor hub is installed on the main shaft also known as low speed shaft. The mechanical energy is transmitted through the drive train (shafts, bearings, and gearbox) to the generator which converts mechanical energy into electrical energy. This conversion is usually assisted by a power convertor system which delivers the power from the generator to the grid. Most of the wind turbine components are enclosed in a nacelle on the top of the tower. (Fig. 2.1)

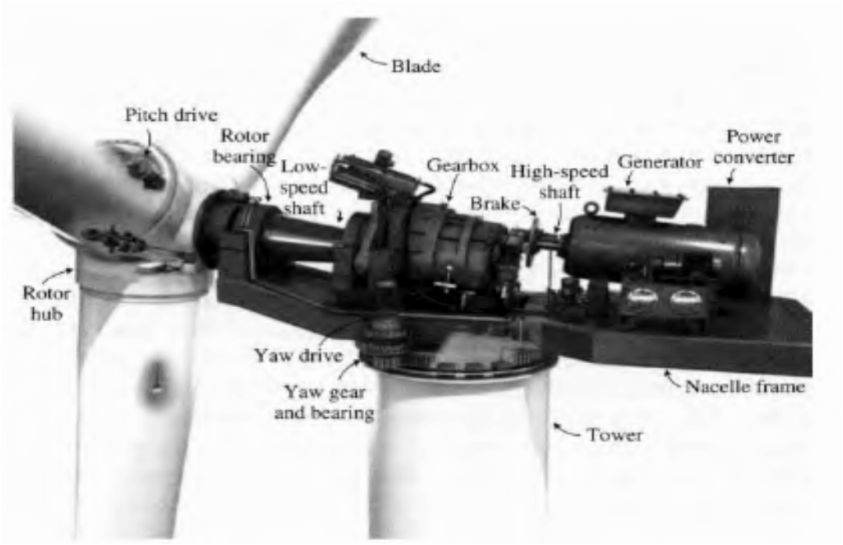

Fig. 2.1 Components of wind energy conversion system

The other parts that are not directly involved in the power conversion, but are important to ensure the proper, efficient and reliable operation of the system include the pitch system, yaw system, mechanical brake, wind speed and direction sensors, power distribution cables, heat dissipation / exchange, lightening protection system, and structural components such as the tower, foundation, and nacelle enclosure. Large WT is also equipped with an uninterruptable power supply or backup energy system that ensures uninterrupted operation of essential part such as the control system, pitch drive, and brakes.

In direct drive (gearless) turbines the absence of the gear box and high speed shaft leads to a more compact drive train and, hence a shorter nacelle. However, the wider diameter of low speed generators requires a taller nacelle structure. This phenomenon is more evident in wound rotor synchronous generators than permanent magnet synchronous generators [52].

2.2 WIND DYNAMICS

The power-speed relations of WT are expressed in the equations:

1. Power in air flow [53]: $P_{air} = 0.5\rho A v^3$ (2.1)

   where P_{air} is power in air flow,
   ρ is air density, Kg/ m^3
   v is velocity of wind. (m/s)
   A is area swept by blade. (m^2)

2. Power Coefficient: $C_P = P_{\text{wind turbine}} / P_{air}$ (2.2)

   $P_{\text{wind turbine}}$ is power of wind turbine. Then we get,

   $P_{\text{wind turbine}} = 0.5\rho A v^3 C_P$ (2.3)

3. Tip speed ratio : $\lambda = \omega r / v$ (2.4)
   where ω = rotational speed of rotor. (rad/sec.)
   r = blade length (m)
   v = upwind speed (m/s)

4. Beta limit: the turbine can never extract more than 59.3% of power of air (P_{air}). Also C_P ranges from 25 to 40 %. Here the value of C_P is 0.28 in model.

C_P & λ are dimensionless and so can be used to describe the performance of any size of WT rotor. Fig. 2.2 shows that the maximum power coefficient is only achieved at a single wind speed. Hence one argument for operating a WT at variable rotation speed is that it is possible to operate at maximum C_P over a range of wind speeds.

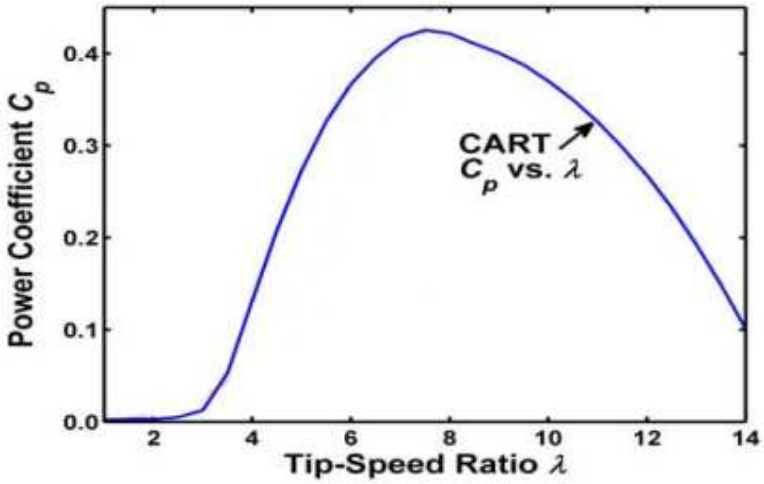

Fig 2.2 Graph for power coefficient versus tip speed ratio

Wind turbine extracts energy from the wind by transferring the thrust force of the air passing through the turbine rotor into the blades. The more kinetic energy a WT pulls out of the wind, the more the wind will be slowed down as it leaves the turbine. If all the energy from the wind is extracted, the air would move away with the speed zero, i.e. the air could not leave the turbine. This power extraction is limited therefore up to 59 % of wind power. This is called as beta limit.

2.3 POWER CHARACTERISTICS OF WIND TURBINE

The power output of a WT at various wind speeds is conventionally described by its power curve. The power curve gives the steady state electrical power output as a function of the wind speed at the hub height and generally measured using 10 min. average data.

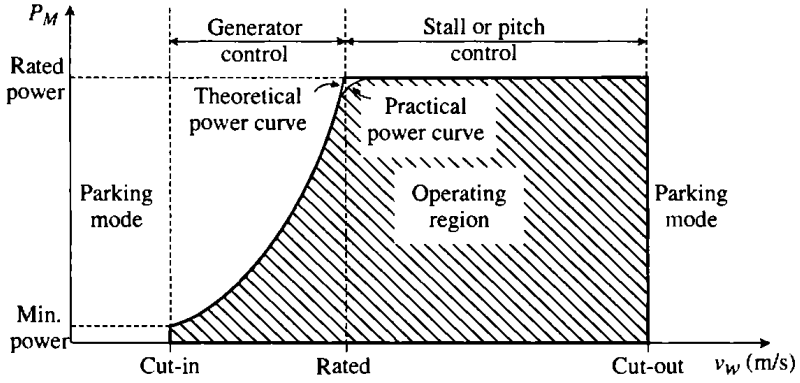

Fig. 2.3 Wind power-speed characteristics

The power has three key points on the velocity scale:

a. Cut-in wind speed - the minimum wind speed at which the machine will deliver useful power.
b. Rated wind speed - the wind speed at which rated power is obtained (rated power is generally the maximum power output of the electrical generator).
c. Cut-out wind speed - the maximum wind speed at which the turbine is allowed to deliver power (usually limited by engineering loads and safety constraints).

Below the cut-in speed, the WT remains shut down as the speed of the wind is too low for useful energy production. Then, once in operation, the power output following a broadly cubic relation with wind speed (although modified by the variation in C_P) until rated wind speed is reached. Above rated wind speed aerodynamic rotor is arranged to limit the mechanical power extracted from the wind and so reduce the mechanical loads on the drive train. Then at very wind speeds the turbine is shut down. The choice of cut-in, rated and cut-out wind speed is made by the WT designer who, for typical wind conditions, will try to balance obtaining maximum energy extraction with controlling the mechanical loads (and hence the capital cost) of the machine.

A typical WT will have an output power that increases as wind speed increases from the cut-in wind speed to the rated wind speed. At the rated wind speed, the generator has reached rated power, and the electrical power must be held constant or reduced for further increases in wind speed [54]. Power curves for existing machines can normally be obtained from the turbine manufacturer. They are found by field measurements, where an anemometer is placed on a most reasonable close to the WT, not on the turbine itself or too close to it, since the turbine may create turbulence and make wind speed measurements unreliable [55].

2.4 FIXED AND VARIABLE SPEED TURBINES

WTs can be classified into fixed-speed and variable-speed turbines [56]. As the name suggests, Fixed-Speed Wind Turbine (FSWT) rotates at almost a constant speed, which is determined by the gear ratio, the grid frequency, and the number of poles of the generator. The maximum conversion efficiency can be achieved only at a given wind speed, and the system efficiency degrades at other wind speeds. The turbine is protected by aerodynamic control of the blades from possible damage caused by high wind gusts. The fixed-speed

turbine generates highly fluctuating output power to the grid, causing disturbances to the power system. This type of turbine also requires a sturdy mechanical design to absorb high mechanical stresses [57].

Also, VSWT (Variable-Speed Wind Turbine) can achieve maximum energy conversion efficiency over a wide range of wind speeds. The turbine can continuously adjust its rotational speed according to the wind speed. In doing so, the tip speed ratio, which is the ratio of the blade tip speed to the wind speed, can be kept at an optimal value to achieve the maximum power conversion efficiency at different wind speeds [58]. To make the turbine speed adjustable, the WT generator is normally connected to the utility grid through a power converter system [56]. The converter system enables the control of the speed of the generator that is mechanically coupled to the rotor (blades) of the WT. As shown in Table 2.1, the main advantages of the variable-speed turbine include increased wind energy output, improved power quality, and reduced mechanical stress [57].

Table 2.1 Advantages and drawbacks of fixed- and variable-speed wind turbines

Speed mode	Advantages	Disadvantages
Fixed speed	Simple, robust, reliable, Relatively low energy-conversion	Low cost and maintenance, efficiency, High mechanical stress, High power fluctuations to the grid
Variable speed	High-energy conversion efficiency, Improved power quality, Reduced mechanical stress	More complex control system, Additional cost and losses due to use of converters

The main drawbacks are the increased manufacturing cost and power losses due to the use of power converters. Nevertheless, the additional cost and power losses are compensated for by the higher energy production. Furthermore, the smoother operation provided by the controlled generator reduces mechanical stress on the turbine, the drive train and the supporting structure. This has enabled manufacturers to develop larger WTs that are more cost-effective. Due to the above reasons, variable-speed turbines dominate the present market [52].

2.5 AERODYNAMIC POWER CONTROL

Turbine blades are aerodynamically optimized to capture the maximum power from the wind in normal operation with a wind speed in the range of about 3 to 15 m/s. In order to avoid damage to the turbine at a high wind speed of approximately 15 to 25 m/s, aerodynamic power control of the turbine is required [59].

The blade rotates in the wind because the air flowing along the surface that is not facing the wind moves faster than that on the surface against the wind. This creates a lift force to pull the blade to rotate. The angle of attack of the blade plays a critical role in determining the amount of force and torque generated by the turbine. Therefore, it is an effective means to control the amount of captured power. There are three aerodynamic methods to control the capture of power for large WTs: passive stall, active stall, and pitch control.

2.5.1 Passive-Stall Control

In passive-stall-controlled WTs, the blade is fixed onto the rotor hub at an optimal (rated) angle of attack. When the wind speed is below or at the rated value, the turbine blades with the rated angle of attack can capture the maximum possible power from the wind. With the wind speed exceeding the rated value, the strong wind can cause turbulence on the surface of the blade not facing the wind. As a result, the lifting force will be reduced and eventually disappear with the increase of the wind speed, slowing down the turbine rotational speed. This phenomenon is called stall. The stall phenomenon is undesirable for airplanes, but it provides an effective means to limit the power capture to prevent turbine damage [58].

2.5.2 Active-Stall Control

In active-stall turbines, the stall phenomenon can be induced not only by higher wind speeds, but also by increasing the angle of attack of the blade. Thus, active-stall WTs have adjustable blades with a pitch control mechanism. When the wind speed exceeds the rated value, the blades are controlled to turn more into the wind, leading to the reduction of captured power. The captured power can, therefore, be maintained at the rated value by adjusting the blade angle of attack [58]. When the blade is turned completely into the wind, the blade loses all interaction with the wind and causes the rotor to stop. This operating condition can be used above the cut-out wind speed to stop the turbine and protect it from damage. With active-stall

control, it is possible to maintain the rated power above the rated wind speed. Active-stall controlled large megawatt WTs are commercially available.

2.5.3 Pitch Control

Similar to the active-stall control, pitch-controlled WTs have adjustable blades on the rotor hub. When the wind speed exceeds the rated value, the pitch controller will reduce the angle of attack, turning the blades (pitching) gradually out of the wind. The pressure difference in front and on the back of the blade is reduced, leading to a reduction in the lifting force on the blade. When the wind is below or at the rated speed, the blade angle of attack is kept at its rated (optimal) value. With higher than the rated wind, the angle of attack of the blade is reduced, causing a reduction in lift force. When the blade is fully pitched, the blade angle of attack is aligned with the wind and no lift force will be produced. The turbine will stop rotating and then be locked by the mechanical brake for protection. The mechanical power of the turbine operating at above the rated wind speed can be tightly controlled.

Both pitch and active-stall controls are based on rotating actions on the blade, but the pitch control turns the blade out of the wind, leading to a reduction in lift force, whereas the active-stall control turns the blades into the wind, causing turbulences that reduce the lift force.

The passive-stall technology was mainly used in the early FSWTs. This technology was further developed into the active-stall technology. The pitch control reacts faster than the active-stall control and provides better controllability. It is widely adopted in today's large wind energy systems.

2.6 MAXIMUM POWER POINT TRACKING (MPPT) CONTROL

The control of a VSWT below the rated wind speed is achieved by controlling the generator. The main goal is to maximize the wind power capture at different wind speeds, which can achieved by adjusting the turbine speed in such a way that the optimal tip speed ratio λ_{opt} is maintained. Fig. 2.4 shows the typical characteristics of a WT operating at different wind speeds, where P_M and ω_M are the mechanical power and mechanical speed of the turbine, respectively. The P_M versus ω_M curves are obtained with the blade angle of attack set to its optimal value. For the convenience of analysis and discussion, the mechanical power, turbine speed, and the wind speed are all expressed in per-unit terms.

For a given wind speed, each power curve has a maximum power point (MPP) at which the optimal tip speed ratio is achieved. To obtain the maximum available power from the wind at different wind speeds, the turbine speed must be adjusted to ensure its operation at all the MPPs. The trajectory of MPPs represents a power curve, which can be described by

$$P_M \alpha (\omega_M)^3 \tag{2.5}$$

The mechanical power captured by the turbine can also be expressed in terms of the torque:

$$P_M = T_M \omega_M \tag{2.6}$$

where T_M is the turbine mechanical torque. Substituting (2.6) into (2.5) yields

$$T_M \alpha (\omega_M)^2 \tag{2.7}$$

The relations between the mechanical power, speed, and torque of a WT can be used to determine the optimal speed or torque reference to control the generator and achieve the MPP operation. Several control schemes have been developed to perform the MPPT, and a brief description of three MPPT methods is given in the next subsections.

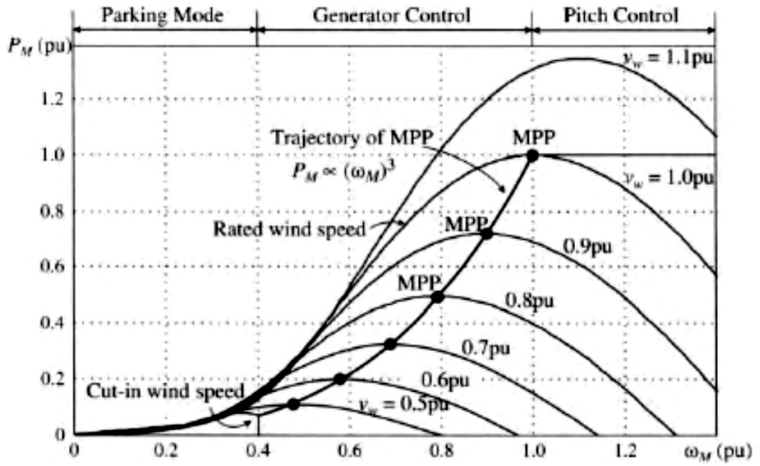

Fig 2.4 Wind turbine power speed characteristics and maximum power point operation

According to the power curve illustrated in Fig. 2.4, the operation of the WT can be divided into three modes: parking mode, generator-control mode, and pitch-control mode:

• Parking mode: When the wind speed is below cut-in speed, the turbine system generates less power than its internal consumption and, therefore, the turbine is kept in parking mode. The blades are completely pitched out of the wind, and the mechanical brake is on.

• Generator-control mode: When the wind speed is between the cut-in and rated speed, the blades are pitched into the wind with its optimal angle of attack. The turbine operates with variable rotational speeds in order to track the MPP at different wind speeds. This is achieved by the proper control of the generator.

• Pitch-control mod: For higher than rated wind speeds but below the cut-out limit, the captured power is kept constant by the pitch mechanism to protect the turbine from damage while the system generates and delivers the rated power to the grid When the wind speed reaches or exceeds the cut-out speed, the blades are pitched completely out of the wind. No power is captured, and turbine speed is reduced to zero. The turbine will be locked into the parking mode to prevent damage from the strong wind [52].

2.7 ISSUES RELATED TO WIND POWER INTERCONNECTION TO GRID

According to grid codes wind farms tend to be considered as power generation plants, which should perform in a similar manner to conventional power generation plants. The main issues related to grid interconnection and operation; include fault-ride through requirements, active-reactive power control, frequency /voltage regulation, power quality and system protection.

2.7.1 Fault-ride through requirements

The increased penetration of wind power into utility grid brings challenges to power converter design in WECSs. Among all, low-voltage ride-through has been enforced in the field, which is a major challenge for WECS [60]. The fault ride-through capability of a WECS is of particular concern because the disconnection of a large wind generator caused by network disturbances may lead to system instability and cascaded failures [61].

Grid disturbance such as voltage dips are caused by short circuit fault can lead to power generating unit disconnected from the grid, which may cause instability in the grid. To avoid this grid code requires power generating units to remain connected and continuously operated even if the voltage dips reaches very low value. The depth and duration of voltage dips are

usually defined by a voltage time diagram. Fig. 2.5 shows LVRT requirements during grid faults, where V_N is the nominal voltage of the grid. Above the limit line a power generating system must remain connected during the faults even when the grid voltage falls to zero with duration of less than 150ms. The system is allowed to disconnect from the grid only when voltage dips are in the area below the limit line [52].

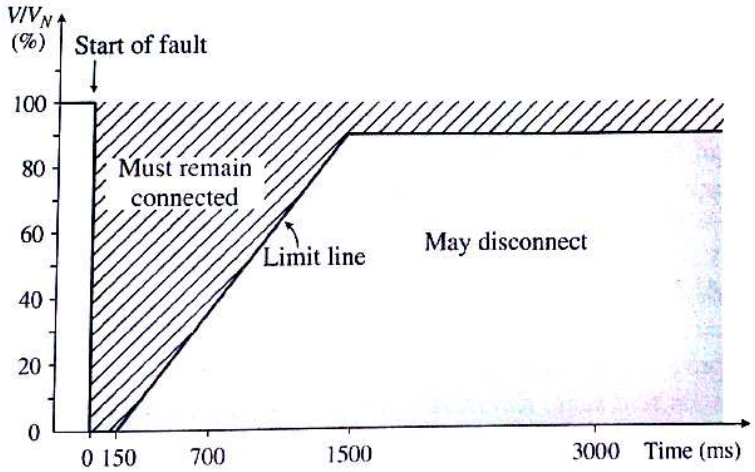

Fig.2.5 Grid requirement for low voltage ride-through

2.7.2 Frequency and Voltage Operating Range

The electrical behaviour of the network, in terms of frequency and voltage, due to its dynamic nature is continuously changing. Generally, these changes occur in very small quantities.

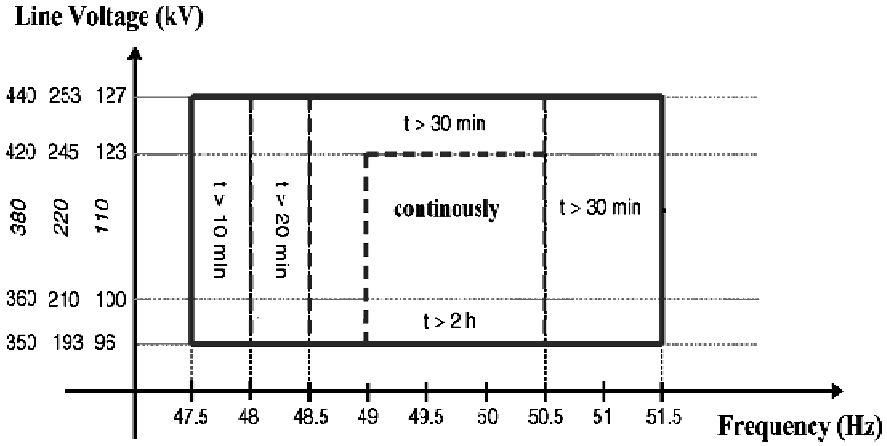

Fig.2.6 Grid code related to frequency

It is a requirement that users of the transmission system are able to continue operating in a normal manner over a specified range of frequency and voltage conditions. With respect to frequency and for a 50Hz system, this would be in the range of 49 to 51Hz. With respect to voltage, this range could be ±10% of the nominal voltage.

Table 2.2 Frequency and voltage tolerance range

	Normal continuous operations	Required	Very short term
Frequency	49-51 Hz	47.5-49Hz and 51-52 Hz	47-47.5 Hz
Voltage	5% tolerance	10% tolerance	

Flicker is induced by voltage fluctuations, which are caused by load flow changes in the grid. Grid connected WTs may have considerable fluctuations in output power, which depends on the wind power generation technology applied [62].

2.7.3 Reactive Power and Voltage Control Capability

Power Factor Control

To minimize losses and thus maintain high levels of efficiency, it is preferable that networks operate with voltage and current in phase that is, the power factor is unity. However, users of electrical systems often tend to have inductive loads or generation facilities that operate such that voltage and current are out-of-phase. In addition, power system components including lines and transformers consume large levels of reactive power. As the behaviour of the network is continuously changing, users are required to have the ability to adjust their reactive power production or consumption, in order that reactive power production and consumption are balanced over the entire network. In most cases, it is the generators who provide this control ability. The range, for example, could be from 0.95 leading to 0.95 lagging. The studied model is operated on power factor control mode in the control schemes incorporated.

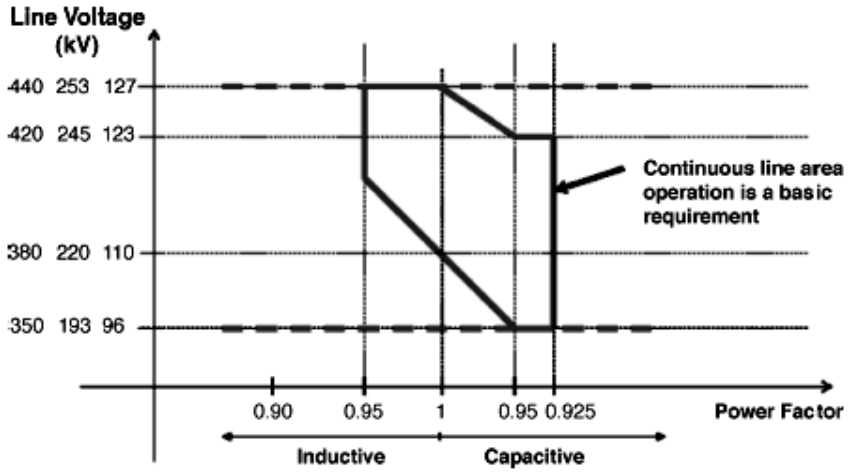

Fig.2.7 Reactive power control as a function of grid voltage

Voltage Support

A generating station adjusts its reactive power production in order to control voltage on the local network. If the network voltage decreases to a level below a predefined range, an installation may be required to supply reactive power to the network to raise the voltage. Conversely, if the network voltage increases to a level above a predefined upper limit, then the installation would be required to consume reactive power to bring the voltage back within acceptable limits. The reactive compensation for FSWT based SCIG wind parks are based on capacitor banks locally connected in each machine [63]. The major problem is that, because of the magnetizing current supplied from the grid to the stator winding, the full load power factor is relatively low [62].

2.7.4 Power control

With respect to wind power, for decreasing wind speed conditions there are limitations in the capabilities of WTs. If the wind speed is falling, a WT may not be able to maintain its output or fully control the rate of decrease of output. However, wind speed profiles can be predicted and so if a controlled ramp down or clearly defined power reduction rate is required, a WTs output can be reduced early, thus reducing the maximum rate of change of output power [64].

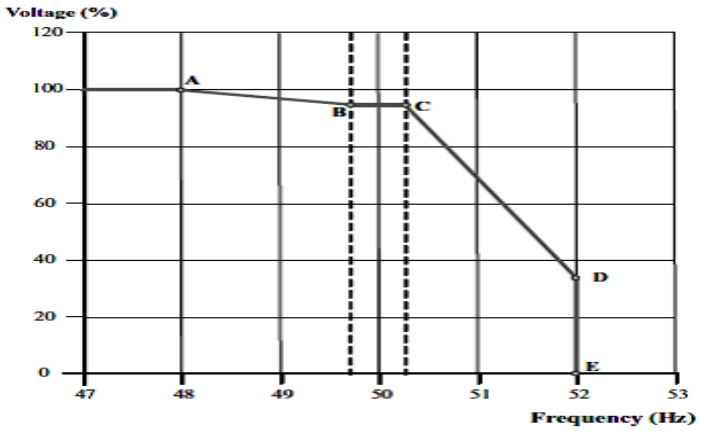

Fig.2.8 Power verses frequency relation

CHAPTER 3

DOUBLY FED INDUCTION GENERATOR

3.1 INTRODUCTION

The DFIG is popular due to inherent characteristics which extend boundary conditions for extracting power from the wind.

Some advantages [12] of DFIG as compared to fixed speed generating are as follows:

1. Reduced inverter cost, because inverter rating is typically 25% of total system power, while the speed range of the Variable speed Generator is ±33% around the synchronous speed.
2. Reduced cost of the inverter filters, because filters are rated for 0.25 p.u. total system power, and inverter harmonics represent a smaller fraction of total system harmonics.
3. Improved system efficiency
4. Power-factor control can be implemented at lower cost, because the DFIG system (four-quadrant converter and induction machine) basically operates similar to a synchronous generator. The converter has to provide only excitation energy.

3.2 COMPONENTS AND OPERATING MODES OF DFIG-BASED WECS

The main components of DFIG based WECS are wound rotor induction generator, aerodynamic system with gear box, rotor side converter, grid side converter, coupling transformer, filter & protection system. The rotor shaft is connected to drive train system of WT and stator terminal is connected to grid.

In the Fig. 3.1 firing control circuit is not shown which generates firing pulse sequence for converters. The converters are operated so as to provide stable operation with the variation of wind speed and fault conditions. Coupling transformer provides electrical isolation between DFIG & grid via mutual coupling. Protection system provides safe operation to converters from heavy transients. The converter system is bidirectional so DFIG can be operated in sub-synchronous and super-synchronous mode. The rotor terminals are connected to back-to-back dc link connected converter system [65]. Power converters for variable-speed drives are classified into direct and indirect converter topologies [66-67]. Further, indirect topologies can be grouped into two main categories: current and voltage source converters [68].

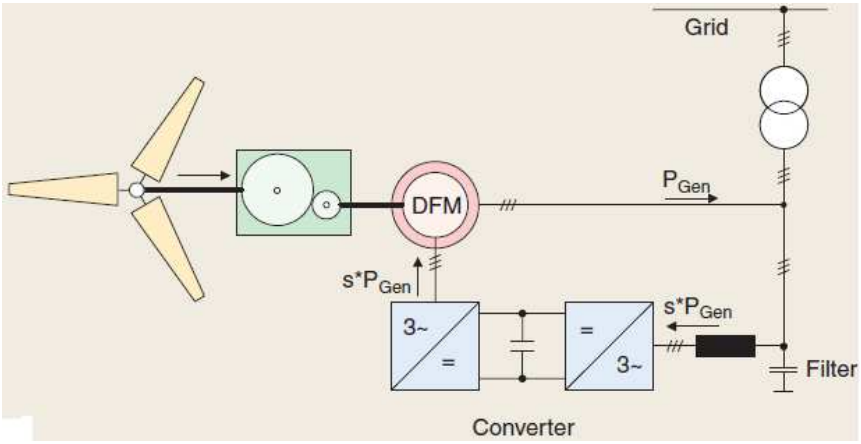

Fig. 3.1 Components of DFIG-based WECS [12]

Control of the varying output voltage and frequency of these induction generators has been made possible by the developments of static power convertors [69]. The insulated gate bipolar transistor (IGBT) is now the main component for power electronics and also for wind-turbine applications [37], but for higher capacity (10 MW), SCR can be used. With the use of converters, the active & reactive power flow through rotor is controlled in both directions. However there are also some problems arising from the use of power converters in wind turbines. Some of the problems [70] are:

1. The converter system can have faults, which means lost production.
2. The efficiency of the converter drops at low power levels
3. The power converters cause harmonic voltages on the grid due to the PWM-modulation.

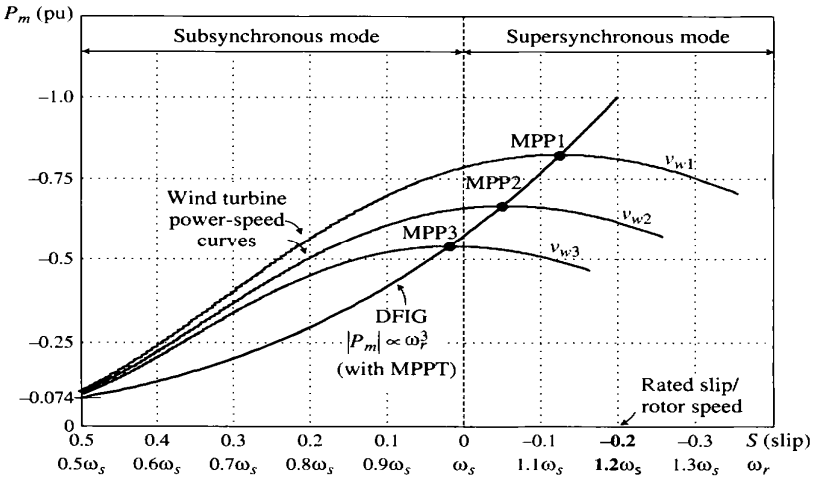

Fig.3.2 Power–speed characteristics in a DFIG wind energy system with MPPT control

Fig. 3.2 shows an example of mechanical power P_m versus slip characteristics of a DFIG WECS. The negative value of mechanical power indicates that the DFIG is in the generating mode. Since the rotor speed of the DFIG is adjustable, one of the MPPT schemes can be implemented to harvest the maximum available power from the WT.

When operating at the MPP on the turbine power-speed curves, ideally, the wind-driven induction generator output should follow the wind cube-law power curve [71].The generator's mechanical power from the shaft P_m is proportional to the cube of the rotor speed ω_r. The rotor speed of the generator in Fig. 3-2 is in the range of $0.5\omega_s$ to $1.2\omega_s$ which corresponds to about 58% of the full speed range (zero to $1.2\ \omega_s$). This speed range is normally sufficient for a wind energy system since the power generated at 42% of the rated speed is 0.074 p.u. (only 7.4% of the rated power) The rated slip at which the rated power (1 pu) is generated (in this example is -0.2), which represents the rated steady state operating point of the system. Dynamically, the DFIG may operate up to a slip of -0.3 p.u. (i.e. 30% above the synchronous speed ω_s). As a consequence, the power converters in the rotor circuit should be designed to handle about 30% of the rated stator power. Depending on the rotor speed, there are two modes of operation in a DFIG based WECS:

1. Super-synchronous mode, in which the generator operates above the synchronous speed
2. Sub-synchronous mode, in which the generator operates below the synchronous speed, as shown in Fig. 3.2.

The slip is negative in the super-synchronous mode and becomes positive in the sub-synchronous mode.

Fig. 3.3 shows the power flow in a DFIG-WECS; the harmonic filter in the rotor circuit and the grid-side transformer are omitted for simplicity. Depending on whether the slip is positive or negative, the rotor circuit can receive or deliver power from or to the grid.

In the super-synchronous operation mode, the mechanical power $|P_m|$ from the shaft is delivered to the grid through both stator and rotor circuits. The rotor power $|P_r|$ is transferred to the grid by power converters in the rotor circuit, whereas the stator power $|P_S|$ is delivered to the grid directly.

For the sub-synchronous operation in Fig. 3.3, the rotor receives the power from the grid. Both mechanical power $|P_m|$ and rotor power $|P_r|$ are delivered to the grid through the stator. Although the stator power $|P_S|$ is the sum of $|P_m|$ and $|P_r|$, it will not exceed its power rating

since in the sub-synchronous mode the mechanical power $|P_m|$ from the generator shaft is lower than that in the super-synchronous mode. As in the previous case, neglecting the losses, the total power delivered to the grid $|P_g|$ is the input mechanical power $|P_m|$.

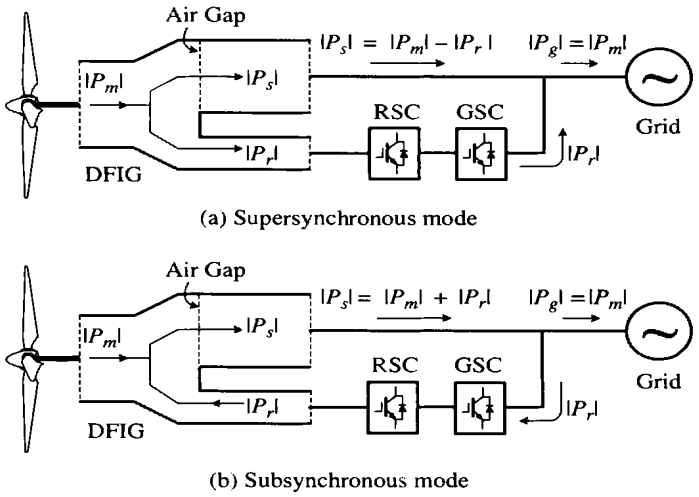

Fig. 3.3 Power flow in a DFIG wind energy conversion system [52]

Since the DFIG generates less power when operating in the sub-synchronous mode, the power rating for the converter is determined by the rated or maximum slip in the super-synchronous mode, in which the converters handle the highest rotor power. For instance, the maximum slip for a DFIG during transients caused by gusts of wind is |–0 .3|, and the power to be processed by the converters is approximately 0.3 of the maximum stator power [52].With the variation of rotor speed, transfer of slip power via the frequency converter can be reversed.

1. In the sub-synchronous operating mode (partial load range) the stator of the DFIG feeds all generated electrical power to the grid, and additionally makes slip power available which is fed from the frequency converter to the rotor via the generator's slip rings.
2. However, in the super-synchronous operating mode (nominal load range) total power consists of the components fed by the stator of the DFIG plus slip power, which is fed from the rotor to the grid via the frequency converter [72].

3.3 DYNAMIC MODELLING OF DFIG

To develop decoupled control of active and reactive power, a DFIG dynamic model is needed. The construction of a DFIG is similar to a WRIM and comprises a three-phase stator

winding and a three-phase rotor winding. The latter is fed via slip rings [76]. The *dq*-axis model of the induction generator can be obtained by decomposing the space vectors into their corresponding d- and q-axis components, that is,

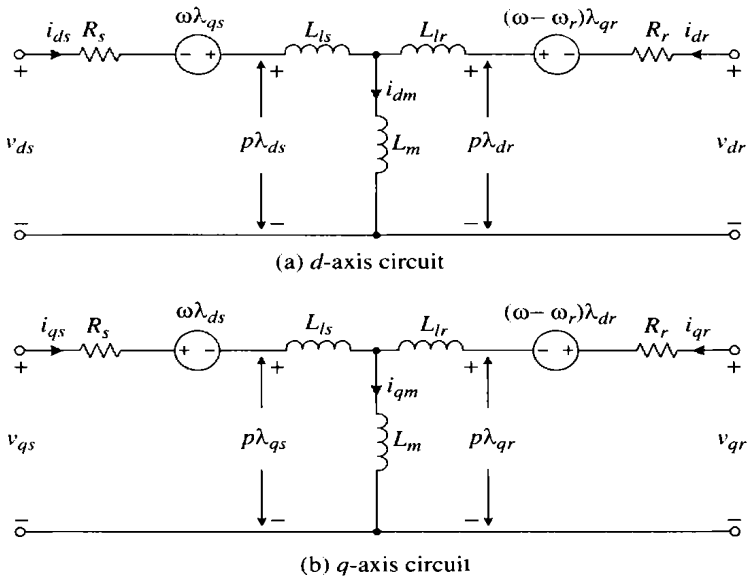

Fig. 3.4 Induction generator *dq* axis model in arbitrary reference frame

$$V_s = V_{ds} + j\,V_{qs}\ ;\ I_s = I_{ds} + j\,I_{qs}\ ;\ \lambda_s = \lambda_{ds} + j\,\lambda_{qs} \tag{3.1}$$

$$V_r = V_{dr} + j\,V_{qr}\ ;\ I_r = I_{dr} + j\,I_{qr}\ ;\ \lambda_r = \lambda_{dr} + j\,\lambda_{qr} \tag{3.2}$$

The dynamics of the DFIG is represented by a fourth-order state space model using the synchronously rotating reference frame (*dq*-frame) as given in (3.3)-(3.6) [16]:

$$V_{qs} = r_s\,I_{qs} + \omega_e\,\lambda_{ds} + d/dt\,(\lambda_{qs}) \tag{3.3}$$

$$V_{ds} = r_s\,I_{ds} - \omega_e\,\lambda_{qs} + d/dt\,(\lambda_{ds}) \tag{3.4}$$

$$V_{qr} = r_r\,I_{qr} + (\omega_e - \omega_r)\,\lambda_{dr} + d/dt\,(\lambda_{qr}) \tag{3.5}$$

$$V_{dr} = r_r\,I_{dr} + (\omega_e - \omega_r)\,\lambda_{qr} + d/dt\,(\lambda_{dr}) \tag{3.6}$$

Where $V_{qs,}$ $V_{ds,}$ $V_{qr,}$ V_{dr} are the q and d-axis stator and rotor voltages, respectively. $I_{qs,}$ $I_{ds,}$ $I_{qr,}$ I_{dr} are the q and d-axis stator and rotor currents, respectively λ_{qs} , λ_{ds} , λ_{qr} , λ_{dr} are the q and d-axis stator and rotor fluxes, respectively. ω_e is the angular velocity of the synchronously rotating reference frame. ω_r is rotor angular velocity, r_s and r_r are the stator and rotor resistances, respectively. The flux linkage equations are given as:

$$\lambda_{qs} = L_s I_{qs} + L_m I_{qr} \tag{3.7}$$

$$\lambda_{ds} = L_s I_{ds} + L_m I_{dr} \tag{3.8}$$

$$\lambda_{qr} = L_m I_{qs} + L_r I_{qr} \tag{3.9}$$

$$\lambda_{dr} = L_m I_{ds} + L_r I_{dr} \tag{3.10}$$

where L_s ,L_r ,L_m and are the stator, rotor, and mutual inductances, respectively, with $L_s = L_{ls} + L_m$ and $L_r = L_{lr} + L_m$: L_{ls} being the self inductance of stator and L_{lr} being the self inductance of rotor. Solving (3.7) - (3.10) in terms of current equations:

$$I_{qs} = \frac{1}{\sigma Ls}\lambda_{qs} - \frac{Lm}{\sigma LsLr}\lambda_{qr} \tag{3.11}$$

$$I_{ds} = \frac{1}{\sigma Ls}\lambda_{ds} - \frac{Lm}{\sigma LsLr}\lambda_{dr} \tag{3.12}$$

$$I_{qr} = \frac{1}{\sigma Lr}\lambda_{qr} - \frac{Lm}{\sigma LsLr}\lambda_{qs} \tag{3.13}$$

$$I_{ds} = \frac{1}{\sigma Lr}\lambda_{dr} - \frac{Lm}{\sigma LsLr}\lambda_{qs} \tag{3.14}$$

Where, leakage coefficient $\sigma = \frac{Ls\,Lr-(Lm.Lm)}{Ls\,Lr}$

The dynamic modelling in state space form is necessary to carry out simulation using different simulation tools such as MATLAB or PSCAD. The basic state space form helps to analyze the system in the transient condition.

According to the basic definition, the space whose co-ordinate axes are the '*n*' state variables with time as the implicit variable is called the state space. The variables of the state space

(state variables) are involved to determine the state of the dynamic system. Basically these are the energy storing elements contained in the system like inductor and capacitor. The fundamental equation of the state space is as follows:

$$X(t) = AX(t) + BU(t)$$

$$Y(t) = CX(t) + DU(t) \tag{3.15}$$

Equation (3.15) is for linear time invariant system, where *A, B, C,* and *D* are state, input, output and feed forward matrices, respectively, *X* is the state vector and *Y* is the output vector. Equation (3.16) is for linear time variant system, where *A, B, C,* and *D* are time dependent matrices.

$$X(t) = A(t)X(t) + B(t)U(t)$$

$$Y(t) = C(t)X(t) + D(t)U(t) \tag{3.16}$$

In the DFIG system, the state variables are normally currents or fluxes. In the following section, the state space equations for the DFIG in synchronously rotating frame has been derived with flux linkages as the state variables. Substituting (3.11) - (3.14) into (3.3) - (3.6) gives the DFIG dynamics in the state space form as:

$$\frac{d}{dt}\lambda_{qs} = -\frac{rs}{\sigma Ls}\lambda_{qs} - \omega_e \lambda_{ds} + \frac{rs\,Lm}{\sigma\,Ls\,lr}\lambda_{qr} + V_{qs} \tag{3.17}$$

$$\frac{d}{dt}\lambda_{ds} = -\frac{rs}{\sigma Ls}\lambda_{ds} + \omega_e \lambda_{qs} + \frac{rs\,Lm}{\sigma\,Ls\,lr}\lambda_{dr} + V_{ds} \tag{3.18}$$

$$\frac{d}{dt}\lambda_{qr} = -\frac{rr}{\sigma Lr}\lambda_{qr} - (\omega_e - \omega_r)\lambda_{dr} + \frac{rr\,Lm}{\sigma\,Ls\,lr}\lambda_{qs} + V_{qr} \tag{3.19}$$

$$\frac{d}{dt}\lambda_{dr} = -\frac{rr}{\sigma Lr}\lambda_{dr} + (\omega_e - \omega_r)\lambda_{qr} + \frac{rr\,Lm}{\sigma\,Ls\,lr}\lambda_{ds} + V_{dr} \tag{3.20}$$

3.3.1 Active Power, Reactive Power and Torque Calculation

All the equations above are induction motor equations. When the induction motor operates as a generator, current direction will be opposite. Assuming negligible power losses in stator and rotor resistances, the active and reactive power outputs from stator and rotor side are given as:

$$P_s = -3/2\ [V_{qs}\, I_{qs} + V_{ds}\, I_{ds}] \quad (3.21)$$

$$Q_s = -3/2\ [V_{qs}\, I_{ds} - V_{ds}\, I_{qs}] \quad (3.22)$$

$$P_r = -3/2\ [V_{qr}\, I_{qr} + V_{dr}\, I_{dr}] \quad (3.23)$$

$$Q_r = -3/2\ [V_{qr}\, I_{dr} - V_{dr}\, I_{qr}] \quad (3.24)$$

The total active and reactive power generated by DFIG is:

$$P_{total} = P_r + P_s \quad (3.25)$$

$$Q_{total} = Q_r + Q_s \quad (3.26)$$

If P_{total} and/ or Q_{total} is positive, DFIG is supplying power to the power grid, else it is drawing power from the grid.

In the induction machine, the electromagnetic torque is developed by the interaction of air-gap flux and the rotor magneto-motive force (mmf). At synchronous speed, the rotor cannot see the moving magnetic field; as a result, there is no question of induced emf as well as the rotor current, so the torque becomes zero. But at any speed other than synchronous speed, the machine will experience torque. That is true in case of motor, where as in case of WT generator; electromechanical torque is provided by means of prime mover which is WT in DFIG-based WECS.

The rotor speed dynamics of the DFIG is given as:

$$\frac{d}{dt}\omega_r = \frac{P}{2J}(T_m - T_e - C_f\,\omega_r) \tag{3.27}$$

where P is the number of poles of the machine, is friction coefficient, J is inertia of the rotor, T_m is the mechanical torque generated by WT, and T_e is the electromagnetic torque generated by the machine which can be written in terms of flux linkages and currents as follows:

$$T_e = 3/2\,[\,\lambda_{qs}\,I_{ds} - \lambda_{ds}\,I_{qs}\,] \tag{3.28}$$

where positive (negative) values of T_e means DFIG works as a generator (motor) [73].

3.4 POWER CONVERTERS

The power converter is made up of a back-to-back converter connecting the rotor circuit and the grid as shown in Fig. 3.4. The converters are typically made up of voltage source inverters equipped with IGBTs provided with freewheeling diodes, which enable a bi-directional power flow. A RL-filter is provided on the GSC output to minimize switching harmonics supplied to the grid.

3.4.1 Rotor Side Converter

The power rating of the rotor side converter (RSC) is determined by two factors, namely maximum slip power and reactive power control capability. The RSC can be seen as a current controlled voltage source converter. The control objective of RSC is to regulate the stator side active power (or rotor speed) and the stator side reactive power independently.

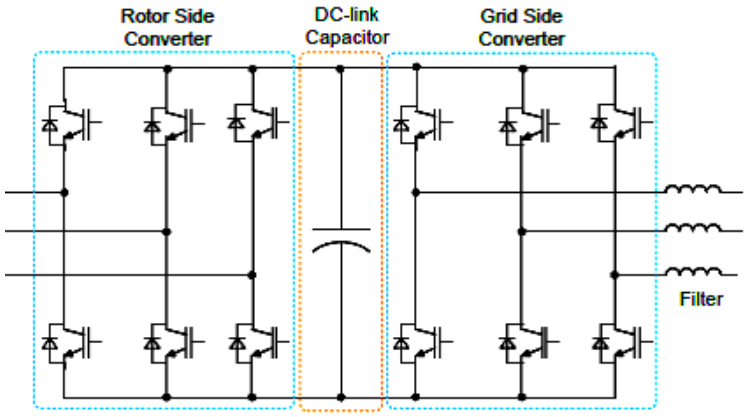

Fig. 3.5 -The ac/dc/ac bidirectional power converter in DFIG

3.4.2 Grid Side Converter

The power rating of the GSC is mainly determined by maximum slip power since it usually operates at a unity power factor to minimize the losses in the converter [74]. The GSC is normally dedicated to controlling the DC-link voltage only. The converter can also be utilized to support grid reactive power during a fault [75]. The grid-side converter can also be used to enhance grid power quality [76]. The amount of energy stored in the dc-link capacitor can be written as:

$$E_c = \int P\, dt = \tfrac{1}{2}\, C\, (V_{DC})^2 \tag{3.28}$$

where P is the net power flow into the capacitor, C is the DC-link capacitor value and V_{DC} is the capacitor voltage. P is equal to $P_r - P_g$, where P_r is the rotor power inflow and P_g is the grid power outflow.

CHAPTER 4

MODELLING AND CONVERTER CONTROL SCHEMES

4.1 SINGLE LINE DIAGRAM & WIND TURBINE MODELLING

The model of DFIG-WECS is developed with back-to-back converters, wind turbine, power system components such as coupling transformer, transmission line, grid, measurement instruments etc. The model has been developed in EMTDC. The single line diagram in the model is as follows:

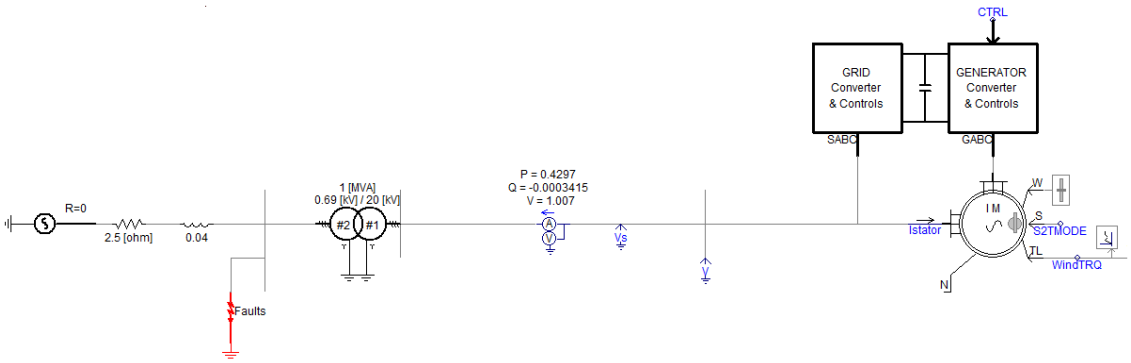

Fig. 4.1 Single line diagram of grid interconnection

The base MVA is 1 p.u. and the generated voltage is set to 20 KV, which is fed to grid via step up transformer. The wind turbine, converter and induction generator modeled are based on p.u. values. Various measurement and graphical monitoring of parameters are incorporated as per need in model. The induction generator is operated in speed control mode and torque control mode by using the switch to torque mode (S2T MODE) signal. Initially it is operated on speed control & then switchover to torque control mode. The speed range of rotor is limited by slider connected to *W* terminal of induction generator. At the secondary side of transformer, 3 phase symmetrical fault is modeled.

The wind turbine model is based on per unit system. The dynamic equations of power and wind relation are modeled. (Fig. 4.2) Actual rating and measurements are input to the overall power equation.

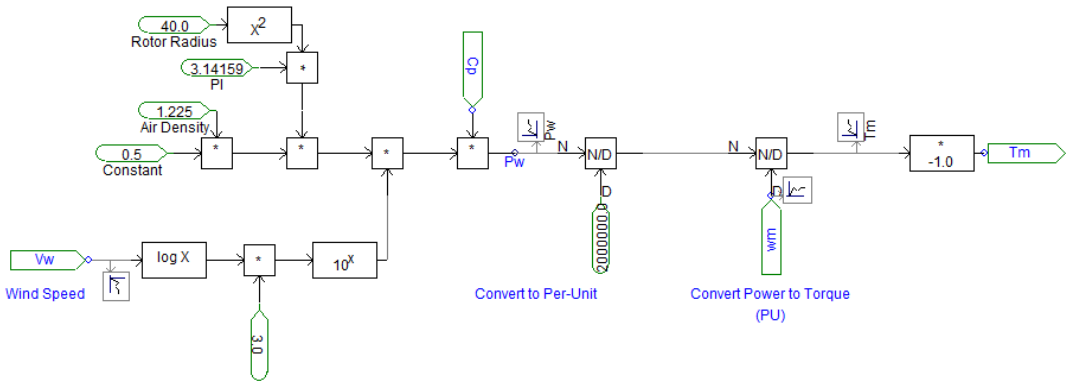

Fig. 4.2 Model of Wind Turbine

Fault Description: The fault is applied to the single line diagram, on the secondary side of the step-up transformer. The fault is applied as:

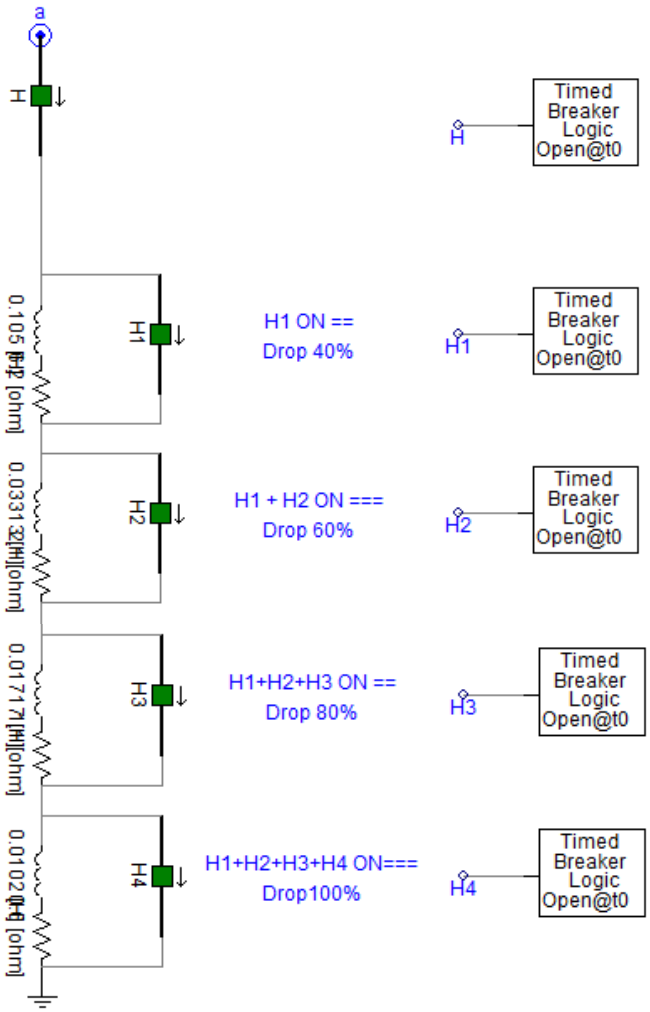

Fig. 4.3 Model of Fault circuit

Table 4.1 Fault status

Time (in sec.)	Status of switch	Status of fault impedance
0 < t < 3	status of H - open	fault impedance are connected
3 < t < 3.2	status of H - close	fault impedance are short circuited
3.2 < t	status of H - open	fault impedance are connected

Fault remains for 3 to 3.2 sec.; the design of fault circuit is stepped type. With the switching of each switch i.e. H1, H2, H3, H4, respectively, the intensity of severity increases.

Each switch can be open/close independently as such, in this model H1, H2 are close at t = 3 sec. and opened at t = 3.2 sec. (Fig. 4.3) The fault severity increases with the short circuiting of impedances from the interconnection. In the model, at normal conditions impedance offer is 14.09 ohm. When H1 & H2 are close or first two impedances Z1 & Z2 are short so as they offer impedance of 2.36 ohm. The drop in the voltage falls near about 60 % in the fault duration.

4.2 MODELLING OF CONTROL SCHEMES

SFO is studied & developed at the generator side, while VOC is employed for the grid side for model [61, 13,12, 77]. The DFIG usually operates in vector control mode based on the PI controllers in a synchronous reference frame to both SFO and VOC frames. Also the DFIG performance with PI controllers is excellent in normal grid conditions, allowing independent control of the grid active and reactive power [51].

4.3 CURRENT REFERENCE–PWM CONTROL

DFIG wind turbine depends not only on the induction generator but also on the control strategies developed using different orientation frames [37]. The induction machine is controlled in a synchronously rotating *dq* axis frame, with the *d*-axis oriented along the stator-flux vector position [22]. The component i_d produces a flux in the air gap which is aligned with the rotating flux vector linking the stator; whereas the component i_q produces flux at right angles to this vector.(Fig. 4.4)

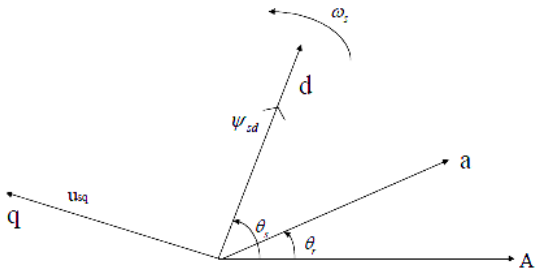

Fig. 4.4 Phasor Diagram of current reference PWM Control [78]

The torque in the machine is the vector cross product of these two vectors, and hence only the component i_q contributes to the machine torque and hence to the power. The component i_d controls the reactive power entering the machine. If i_d and i_q can be controlled precisely, then so can the stator side real and reactive powers [79].

In this way, a decoupled control between the electrical torque and the rotor excitation current is obtained. The rotor-side PWM converter provides the actuation, and the control requires the measurement of the stator and rotor currents, stator voltage and the rotor position. There is no need to know the rotor-induced EMF, as is the case for the implementation with naturally commutated converters. Since the stator is connected to the grid, and the influence of the stator resistance is small, the stator magnetizing current I_{ms} can be considered constant. Under SFO, the relationship between the torque and the *dq* axis voltages, currents and fluxes (all scaled to be numerically equal to the AC per-phase values) may be written as: [22]

$$V^*_{dr} = R_r I_{dr} + \sigma L_r \, dI_{dr}/dt - \omega_{slip} \sigma L_r I_{qr} \tag{4.1}$$

$$V^*_{qr} = R_r I_{qr} + \sigma L_r \, dI_{qr}/dt + \omega_{slip}(L_m I_{ms} + \sigma L_r I_{dr}) \tag{4.2}$$

$$T_e = -3p \, L_m I_{ms} I_{qr} / 2 \tag{4.3}$$

$$\omega_{slip} = \omega_e - \omega_r \tag{4.4}$$

where

σ = leakage factor

L_m , L_r = machine inductances per phase.

P = pole pair

ω_{slip} ,ω_e ,ω_r = supply, rotor, slip angular frequency

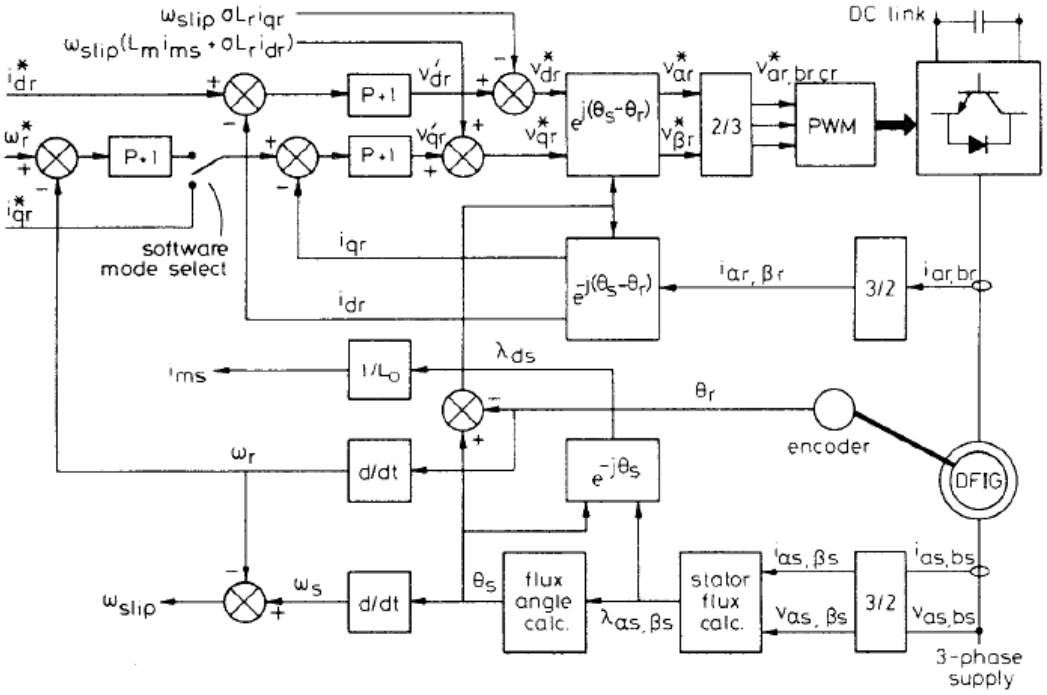

Fig. 4.5 Block diagram of rotor side converter control scheme [22]

There is an approximation considered in the model as compared to block diagram, (Fig. 4.5) the $\omega_{slip}\sigma L_r I_{qr}$ component is neglected from expression of V_{dr}. By this approximation, rotor excitation current I_{dr} is controlled using V_{dr}. The d-axis reference is Reactive power reference Q_g* in model instead of I_{dr}*. Assuming that all reactive power to the machine is supplied by the stator, Reactive power reference Q_g* or I_{dr}* may set to zero. The approximated expression for d- axis is:

$$V^*_{dr} = V'_{dr} = R_r I_{dr} + \sigma L_r \, dI_{dr}/dt \tag{4.5}$$

Similarly the $\omega_{slip}(L_m I_{ms} + \sigma L_r I_{dr})$ is neglected from expression of V_{qr}. By this approximation, the torque is proportional to I_{qr} and I_{qr} can be regulated using V_{qr}. The reference *q*-axis rotor current can be obtained either from outer speed-control loop or from a reference torque imposed on the machine. These two options may be termed as speed-control mode or torque-control mode for the generator. In this model, first speed control mode is applied for 0 to 0.5 sec. and then torque control mode is enabled. The *q*-axis reference W_{ref} is considered in model instead of $I_{qr.}$ The approximated expression for *d*- axis is:

$$V^*_{qr} = V'_{qr} = R_r I_{qr} + \sigma L_r \, dI_{qr}/dt \qquad (4.6)$$

In model, as current reference PWM is applied, rotor current is split into two orthogonal components, *d* and *q*. The voltage V^*_{dr} *(*or V'_{dr} *)* and V^*_{qr} or *(*V'_{qr} *)* are replaced & modeled as I_{rd} and I_{rq}.

In the d-axis model Q_g* is set to 0 p.u. and the Q_g is the reactive power which is supplied to the grid. The reactive power control the voltage magnitude and power factor at grid within limits, the reactive power is considered to be input to comparator. They both are compared and after PI controller defines the accurate instantaneous value of $I_{rd.}$, it controls reactive power $Q_{g.}$

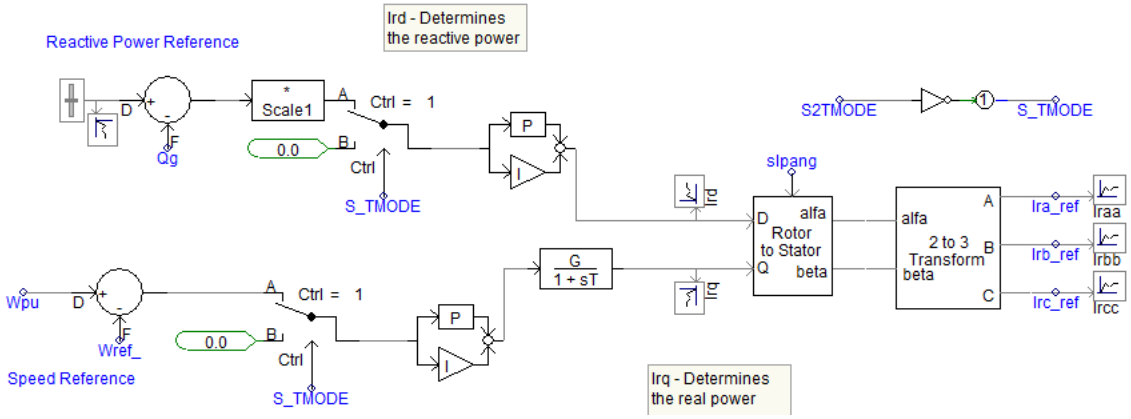

Fig. 4.6 Model of generation of reference currents in RSC

The *q* component of the current is used to regulate the torque. The purpose of the torque controller is to modify the electromagnetic torque of the generator according to wind speed variations and drive the system to the required active power operating point reference. For a measured rotor speed, the reference torque is evaluated by the wind turbine characteristic (for maximum power extraction). Now reference torque is manipulated to generate a reference value for the rotor current I_{rq} in the *q* axis [55].

As the current reference PWM is applied here, rotor voltage reference V^*_{qr} is replaced by rotor current reference I_{rq}. (Fig. 4.6) In q- axis model, speed reference speed $\omega_{ref\_}$ is set to 1.05 p.u. and ω, is rotor speed and operating mode is super-synchronous. Both speeds of rotor are input to the comparator because the model is operated in torque control mode and to maintain constant torque and variable active power, rotor speed is only variable quantity. The

difference in the rotor speed ω, from the reference value, $\omega_{ref\_}$, forms the error signal that is processed by the PI compensator to produce the rotor current $I_{rq.}$

The procedure to obtain correct values of I_{rd} and I_{rq} flowing in the rotor circuit is achieved by generation of corresponding phase reference currents *Ira_ref*, *Irb_ref* and *Irc_ref* followed by a suitable voltage sourced converter based current source to force these currents into the rotor. The latter action is straightforward and can be achieved using current-reference pulse width modulation (CR-PWM). The crucial step is to obtain the instantaneous position of the rotating flux vector in space in order to obtain the rotating reference frame. This can be achieved by realizing that on account of Lenz's law of electromagnetism, the stator voltage (after subtracting rotor resistive drop) is simply the derivative of the stator flux linkage λ_a as in eqn. 4.7 which is written for phase a.

$$v_a - i_a R_a = \frac{d\lambda_a}{dt} \tag{4.7}$$

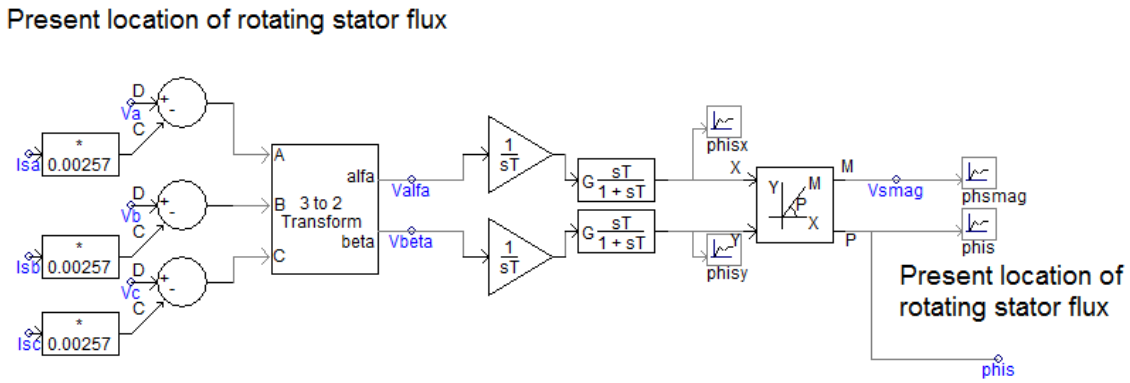

Fig. 4.7 Model of determination of stator flux angle

The control structure can thus be used to determine the location (ϕ_s) or *phis* of the rotating flux vector. The three phase stator voltages (after removal of resistive voltage drop) are converted into the Clarke (α and β) components v_α and v_β, which are orthogonal in the balanced steady state. This transformation is given by:

$$\begin{pmatrix} v_\alpha \\ v_\beta \end{pmatrix} = 2/3 \begin{pmatrix} 1 & -1/2 & -1/2 \\ 0 & \sqrt{3}/2 & -\sqrt{3}/2 \end{pmatrix} \begin{pmatrix} v_a \\ v_b \\ v_c \end{pmatrix} \tag{4.8}$$

Integrating v_α and v_β, we obtain λ_α and λ_β, the Clarke components of stator flux. Converting to polar form

$$|\lambda| = \sqrt{\lambda_\alpha^{\,2} + \lambda_\beta^{\,2}}, \quad \phi_s = \tan^{-1}(\lambda_\beta / \lambda_\alpha) \tag{4.9}$$

The angle *phis* (ϕ_s) give the instantaneous location of the stator's rotating magnetic field. In practical control circuits, some filtering is required in order to rid the quantities λ_α and λ_β of any residual dc component introduced in the integration process. In the model, ϕ_r is measured by the induction generator itself, which is a important component of single line diagram. The parameters measured by it are T_m T_e ω and ϕ_r.. Now the rotor itself is rotating and is instantaneously located at angle ϕ_r (labeled "theta" in the Fig. 4.8). Thus, with a reference frame attached to the rotor, the stator's magnetic field vector is at location $\phi_s - \phi_r$, which we refer to the "slip angle" ϕ_{slip}.

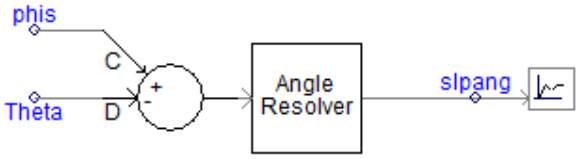

Fig. 4.8 Model of determination of slip angle

The instantaneous values for the desired rotor phase currents *Ira_ref*, *Irb_ref* and *Irc_ref* can be readily calculated using the inverse *dq* transformation, with respect to slip angle. (Fig. 4.3) Once the reference currents are determined, the output rotor phase currents are forced to synthesize similar waveforms as that of reference currents. It is synthesized by using a voltage sourced converter (RSC) operated with current reference pulse width modulation. (Fig. 4.9) [79].

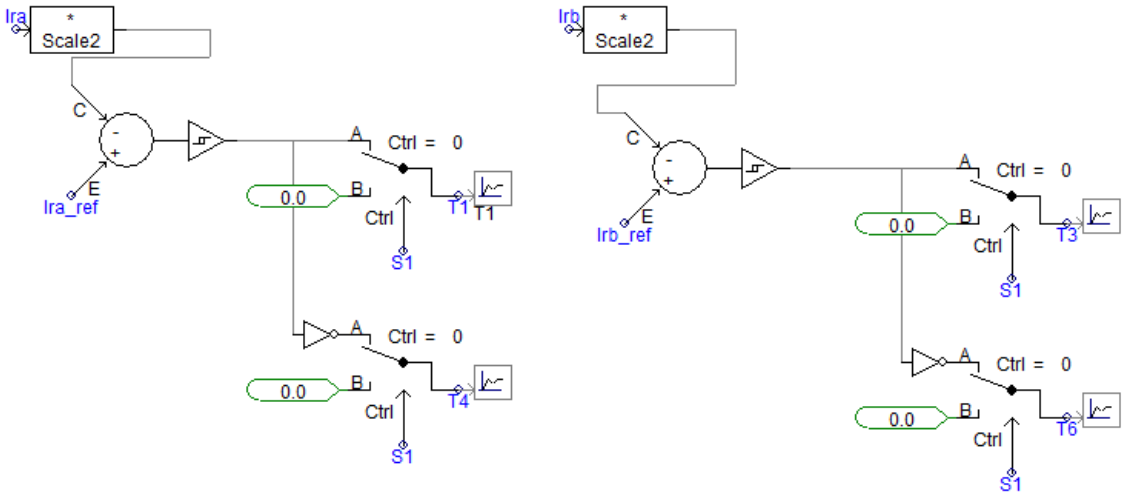

Fig. 4.9 Model of Rotor Side Converter PWM

In the model (Fig. 4.9), the converter firing sequence of RSC is generated. The t_1 and t_4 are fired in consecutive order to control the tracking of *Ira_ref*. Switch t_1 makes the positive ramp function I_1 is generated. (Fig. 4.10) When I_1 reaches upper band value, the t_4 is triggered and t_1 is turned off. Now the I_1 drops linearly until it reaches the lower threshold value. In this way the desired reference *Ira_ref* is synthesized within current limits. Similarly I_b and I_c are also synthesized. It is to control I_d and I_q component and further control reactive power and rotor speed to achieve stable system.

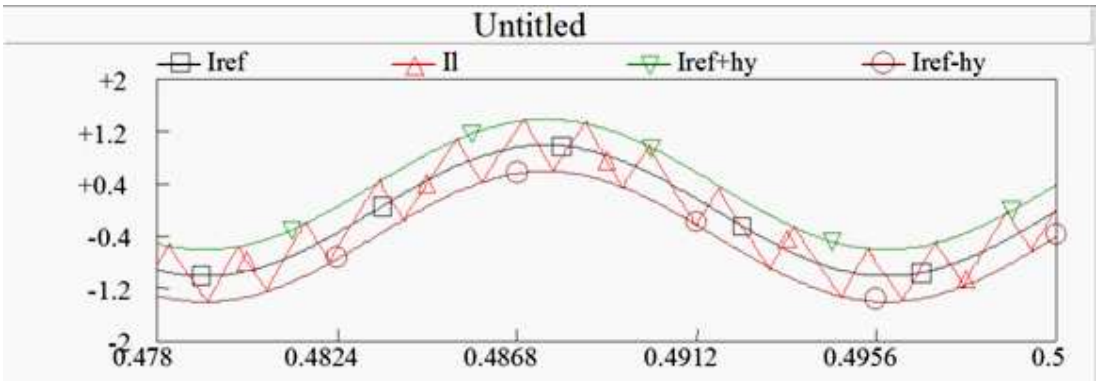

Fig. 4.10 Rotor phase current tracking reference rotor phase current.

4.4 VOLTAGE ORIENTED CONTROL

The objective of the supply-side converter is to keep the DC-link voltage constant regardless of the magnitude and direction of the rotor power. Here vector-control approach is incorporated, with a reference frame oriented along the stator (or supply) voltage vector position, enabling independent control of the active and reactive power flowing between the supply and the supply-side converter. The PWM converter in block diagram is current regulated, with the direct axis current used to regulate the DC-link voltage and the q-axis current component used to regulate the reactive power.

This scheme (Fig. 4.11) is based on transformation between the *abc* stationary reference frame and *dq* synchronous frame. The control algorithm is implemented in the grid-voltage synchronous reference frame, where all the variables are of DC components in steady state. This facilitates the design and control of the inverter. To realize the VOC, the grid voltage is measured and its angle θ_g is detected for the voltage orientation. This angle is used for the transformation of variables from the *abc* stationary frame to the *dq* synchronous frame or vice versa. Various methods are available to detect the grid voltage angle θg.

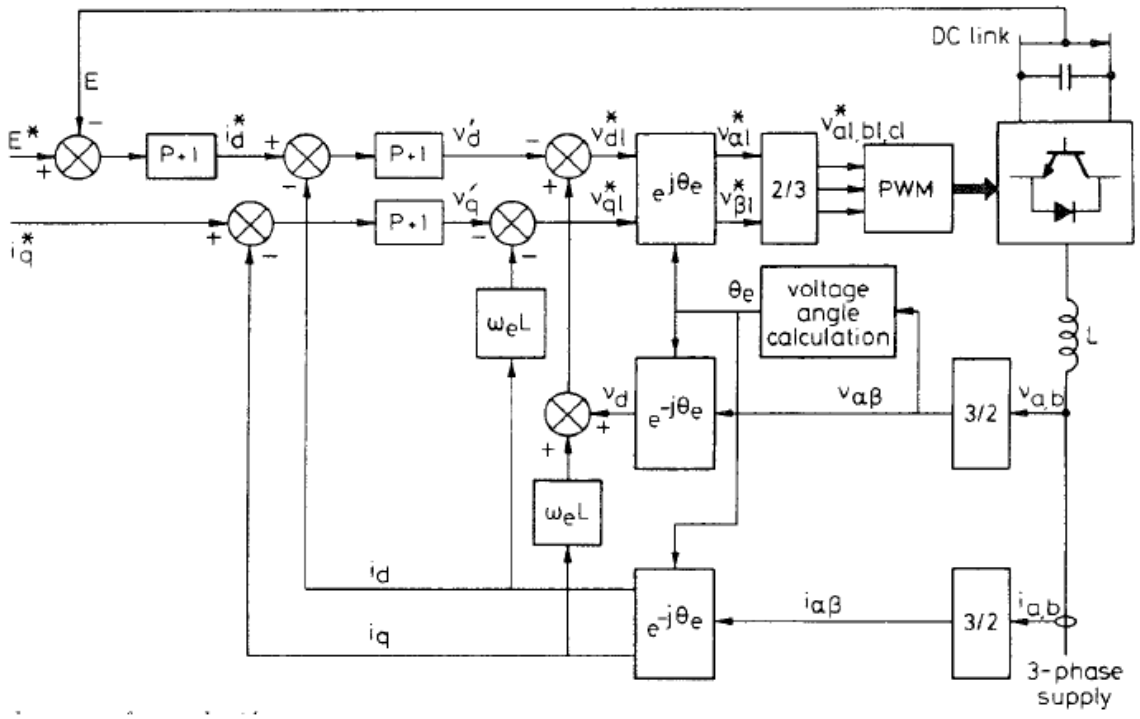

Fig. 4.11 Block diagram of Grid Side Converter control scheme [22]

Assuming that the grid voltages, V_a ,V_b ,V_c are three-phase balanced sinusoidal waveforms, θ_g can be obtained by

$$\theta_g = tan^{-1} (V_{beta} / V_{alpha}) \quad (4.10)$$

where V_{alpha} and V_{beta} can be obtained by the *abc /αβ* transformation (Fig. 4.11) :

$$V_{alpha} = 2/3 [V_a – ½*V_b – ½V_c] \ ; \quad (4.11)$$

$$V_{beta} = 2/3 [\sqrt{3} /2*V_b – \sqrt{3} /2*V_c] \quad (4.12)$$

for $V_a + V_b + V_c = 0$.

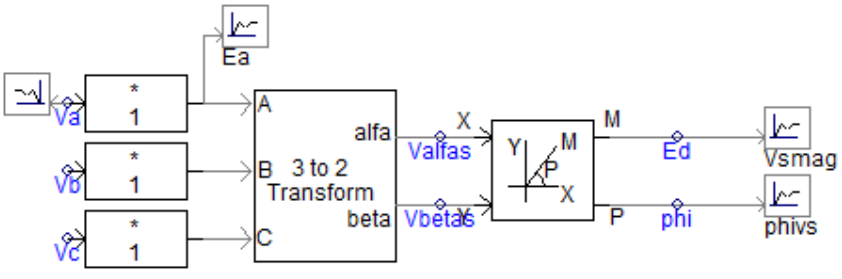

Fig. 4.12 Determination of stator phase angle in GSC

The above equation indicates that there is no need to measure the phase-*c* grid voltage V_c. In practice, the grid voltage may contain harmonics and be distorted, so digital filters or PLLs may be used for the detection of the grid voltage angle θ_g *(phi)*.

There are three feedback control loops in the system: two inner current loops for the accurate control of the *dq*-axis currents i_{1d} and i_{1q}, and one outer DC voltage feedback loop for the control of DC voltage E_{cap}. With the VOC scheme, the three-phase line currents in the *abc* stationary frame i_{1a}, i_{1b}, and i_{1c} are transformed to the two-phase currents i_{1d} and i_{1q} in the *dq* synchronous frame (Fig. 4.13), which are the active and reactive components of the three-phase line currents, respectively. The independent control of these two components provides an effective means for the independent control of system active and reactive power.

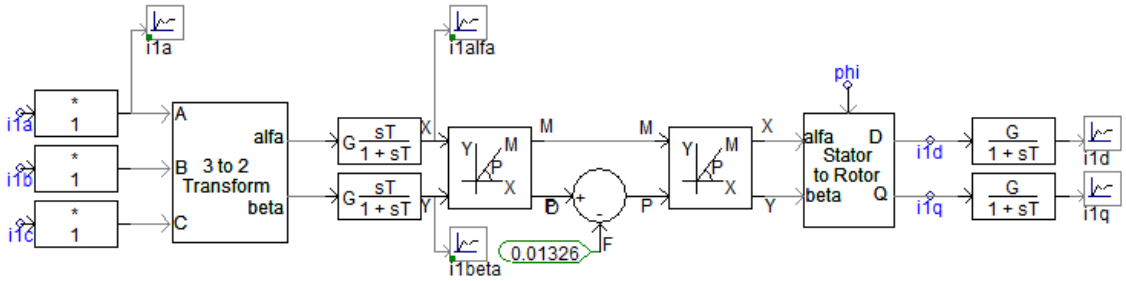

Fig. 4.13 Determination of *dq* stator current

To achieve the VOC scheme, the *d*-axis of the synchronous frame is aligned with the grid voltage vector, therefore *d*-axis grid voltage is equal to grid voltage magnitude $V_{dg} = V_g$ and the resultant *q*-axis voltage V_{qg} is then equal to zero ($V_{qg} = \sqrt{(V_g^2 - V_{dg}^2)} = 0$, from which the active and reactive power of the system can be calculated by

$$P_g = 3/2\,[V_{dg} * i_{1d} - V_{qg} * i_{1q}];\; P_g = 3/2\,[V_{dg} * i_{1d}] \tag{4.13}$$

$$Q_g = 3/2\,[V_{qg} * i_{1d} - V_{dg} * i_{1q}];\; Q_g = 3/2\,[-V_{dg} * i_{1q}] \qquad \text{for } V_{qg} = 0 \tag{4.14}$$

The *q*-axis current reference i_{qref}* can then be obtained from

$$i_{qref}* = Q_g* / (-1.5* V_{dg}) \tag{4.15}$$

where Q_g* is the reference for the reactive power, which is set to negative value for leading power factor operation, or a positive value for lagging power factor operation. The *d*-axis current reference i_{dref*}, which represents the active power of the system, is generated by the PI controller for DC voltage control. On the other hand, when the inverter operates in steady

state, the DC voltage E_{cap} of the inverter is kept constant at a value set by its reference voltage E_{capref}. Neglecting the losses in the inverter, the active & reactive power expression on the AC side of the inverter is equal to the DC-side power as

$$P_g = 3/2\ [V_{dg} * i_{1d}] = E_{cap} * i_{1d} \quad (4.16)$$

$$Q_g = 3/2\ [-V_{dg} * i_{1q}] \quad (4.17)$$

As mentioned earlier, the power flow of the inverter system is bidirectional. When the active power is delivered from the grid to the DC circuit, the converter operates in a rectifying mode $(P_g > 0)$, whereas when the power is transferred from the DC circuit to the grid $(P_g < 0)$, the converter is in an inverting mode. In the model, the power flow will be in inverter mode of Voltage Source Converter. The magnitude of power flow is controlled by $E_{cap.}$ The average DC voltage E_{cap} of the inverter is set by its reference E_{capref} and is kept constant by the PI controller, the direction of the power flow is set by the difference between E_{cap} and E_{capref} according to the following conditions.

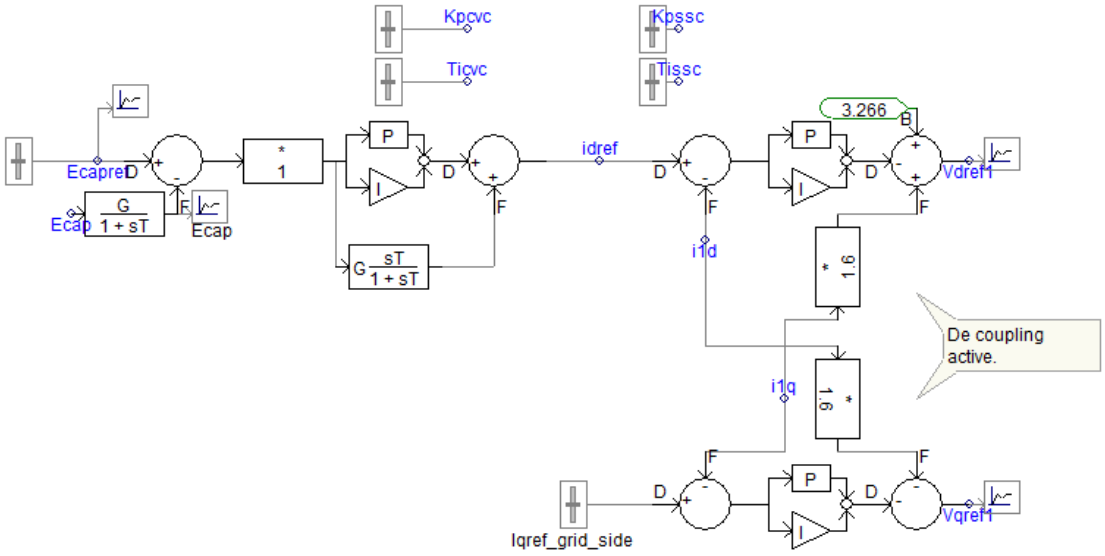

Fig. 4.14 Model of generation of reference *dq* voltages

Table 4.2 Modes of grid side converter for the variation of DC link voltage

$E_{cap} < E_{capref}$	$I_{1d}>0$	$P_g > 0$	Power from grid to load (rectifying mode)
$E_{cap} > E_{capref}$	$I_{1d}<0$	$P_g < 0$	Power from load to grid (inverting mode)
$E_{cap} = E_{capref}$	$I_{1d} = 0$	$P_g = 0$	No power flow between the DC circuit and the grid

The selection of *idref* for the grid side converter is through the control circuit, which attempts to keep the capacitor voltage at its rated value by adjusting the amount of real power. The reactive power order is dialed in, but could have been generated by a similar controller whose objective would be to keep the ac voltage at some set point.

To determine an appropriate DC voltage reference E_{capref}*, system transients and possible grid voltage variations are taken in account. When the inverter operates under the rated conditions, the modulation index m_a is 0.85. The DC reference voltage can then be set by

$$E_{capref}* = \sqrt{6} * V_{ai1} / m_a \quad (4.18)$$

Here E_{capref}* is approximated to 0.8 p.u. This gives around a 25% voltage margin for adjustment during the transients and grid voltage variations.

In the selected circuit, the grid transformer voltage rating is 0.69 kV (supply side), 1 MVA with 10% leakage, giving an impedance ωL = 1.6 **Ω**. Similarly a line-line voltage of 0.69 kV gives a line to neutral voltage of 0.69/√3 KV, and as in the *dq* conversion, peak magnitude v_{dref1} = (0.69/√3)√2 KV = 0.56 kV. The detection of the ac grid voltage reference angle and the generation of *d* and *q* components of current are done in a straightforward manner using a *d-q* transformation.

A dc capacitor is used in order to remove ripple and keep the dc bus voltage relatively smooth. This grid PWM Converter is operated so as to keep the dc voltage on the capacitor at a constant value. It is possible to control the *d* axis current by controlling the *d*-component of the SPWM output waveform and the *q* axis current by *q* component. However, this leads to a poor control system response, because attempting to change i_d also causes i_q to change transiently. Hence, modifications have to be made to the basic PI controller structure so that a decoupled response is possible and a request to change i_d changes i_d and not i_q and vice-versa.

Decoupling in VOC

To further investigate the VOC scheme, the state equation for the grid-side circuit of the inverter in the *abc* stationary reference frame can be expressed as

$$di_{1a} / dt = (V_a - V_{ai}) / L_g \quad (4.19)$$

$$di_{1b} / dt = (V_b - V_{bi}) / L_g \quad (4.20)$$

$$di_{1c} / dt = (V_c - V_{ci}) / L_g \quad (4.21)$$

The above equations can be transformed into the *dq* synchronous reference frame

$$di_{1d} / dt = (V_d - V_{dref1} + \omega_g L_g i_{1q}) / L_g \quad (4.22)$$

$$di_{1q} / dt = (V_q - V_{qref1} + \omega_g L_g i_{1d}) / L_g \quad (4.23)$$

Here ω_g is the speed of the synchronous reference frame, which is also the angular frequency of the grid, and ($\omega_g L_g i_{1q}$ and $\omega_g L_g i_{1d}$ are the induced speed voltages due to the transformation of the three-phase inductance L_g from the stationary reference frame to the synchronous frame.

The derivative of the *d*-axis line current i_{1d} is related to both *d*- and *q*-axis variables, as is the *q*-axis current i_{1q}. This indicates that the system control is cross-coupled, which may lead to difficulties in controller design and unsatisfactory dynamic performance. To solve the problem, a decoupled controller is implemented. (Fig. 4.15)

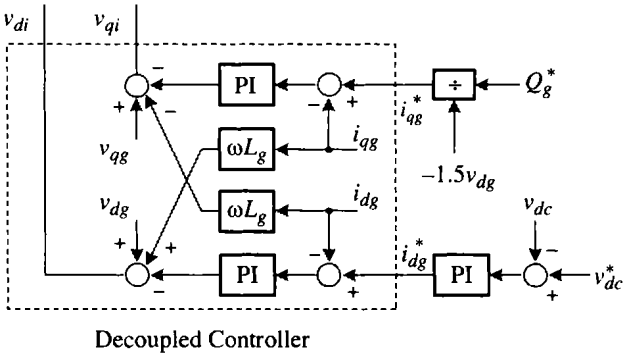

Fig. 4.15 Block diagram of decoupling controller

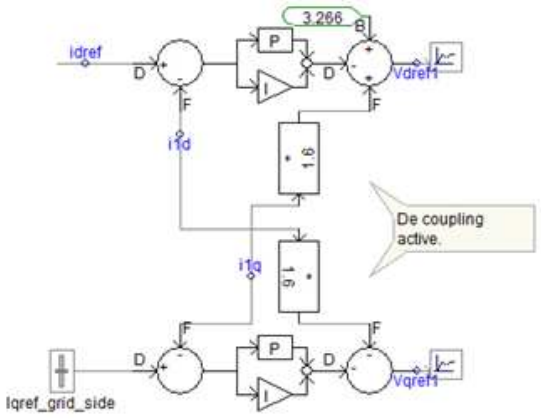

Fig. 4.16 Model of decoupling controller

Assuming that the controllers for the *dq*-axis currents in Fig. 4.16 are of the PI type, the output of the decoupled controller can be expressed as

$$V_{dref1} = -(k_1+k_2/S)(i_{dref} - i_{1d})/L_g + \omega_g L_g i_{1q} + V_d \quad (4.24)$$

$$V_{qref1} = -(k_1+k_2/S)(i_{qref} - i_{1q})/L_g - \omega_g L_g i_{1d} + V_q \quad (4.25)$$

where (k_1+k_2/S) is the transfer function of the PI controller.

Substituting eq-3 in eq-2, we get

$$di_{1d}/dt = (k_1+k_2/S)(i_{dg}^* - i_{dg})/L_g \quad (4.26)$$

$$di_{1q}/dt = (k_1+k_2/S)(i_{qg}^* - i_{qg})/L_g \quad (4.27)$$

The above equation indicates that the control of the *d*-axis grid current i_{dg} is decoupled, involving only *d*-axis components, as is the *q*-axis current i_{qg}. The decoupled control makes the design of the PI controllers more convenient, and the system is more easily stabilized [52].

If these reference voltages Vd_{ref1} and Vq_{ref1} are applied at the secondary of the transformer, the desired currents *idref* and *iqref* will flow in the circuit (Fig. 4.17). The remaining parts of the controls are standard PWM controls. The control blocks convert the above references to phase and magnitude, taking care to limit the magnitude to the maximum rating of the grid side voltage source converter. The reference for each of the three phase voltages is then generated by an inverse *dq* transformation.

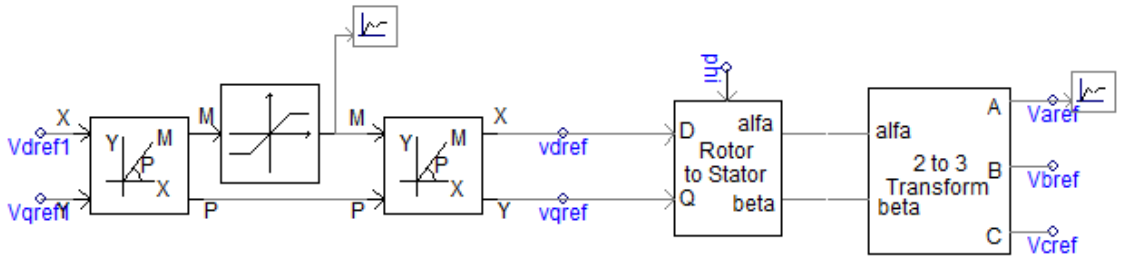

Fig. 4.17 Generation of voltage reference

At Last, a standard sinusoidal PWM controller is considered (Fig. 4.18) for firing pulse generation, in which each of the phase voltages is compared with a high frequency triangle wave to determine the firing pulse patterns for Grid side converter.

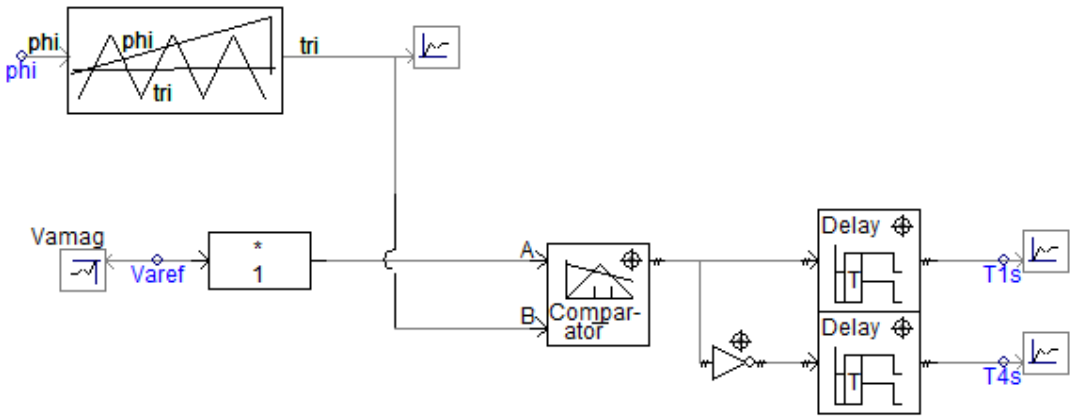

Fig. 4.18 Model of generation of firing pulses by PWM

4.5 CROWBAR PROTECTION

Wind power generation using an induction machine has in fact very fragile characteristic against voltage drop. To address this problem and meet the Fault ride through (FRT) requirements, there should be certain utility to compensate low voltage or certain control technology that can protect the devices while maintaining the rotor's the excitation of wind power generator. So, since this is too burdensome economically, FRT can be for efficient used utilizing crowbar [80].

In wind turbines, the crowbar is installed at the rotor terminals. This prevents overvoltage induced in the case of voltages dips from damaging the rotor converter. It is activated when an anomalous situation is detected (overcurrent in the rotor, overvoltage in the DC link, or low stator voltage).

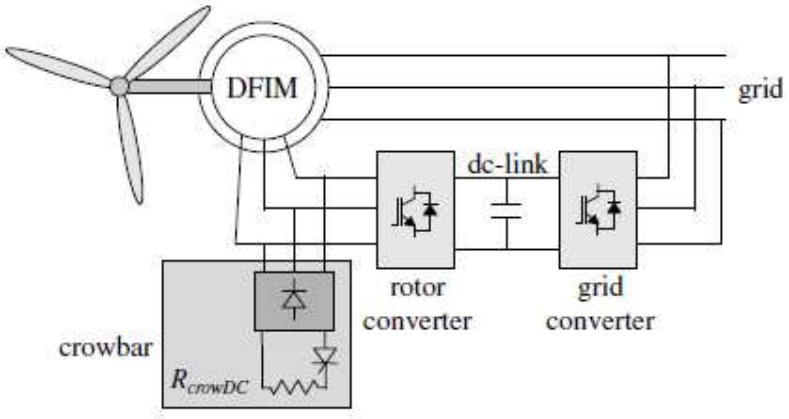

Fig. 4.19 Crowbar interconnection to the grid

The rotor current is then diverted to the crowbar and the rotor converter is switched off. (Fig. 4.19) The crowbar use thyristors (or SCRs) as switches. However, the problem with thyristors was that their cut-off is not controlled: once the crowbar is triggered, it remains connected until the circuit breaker of the generator stops the short-circuit current. As a result, the wind turbine is disconnected from the grid and stops generating electric power even if the grid recovers its normal operation.

In order to provide the LVRT capability, the crowbar short-circuit has to be eliminated without disconnecting the turbine from the grid. The “active crowbar” used in model, in which the activation and also the deactivation can be actively controlled. Modern versions of active crowbars are usually based on the scheme (as shown in Fig. 4.20) and include at least one switch with cut-off capability, such as a GTO or IGBTs. This design allows direct disconnection of the crowbar and instant rotor converter reactivation, enabling the resumption of normal operation in the turbine [64].

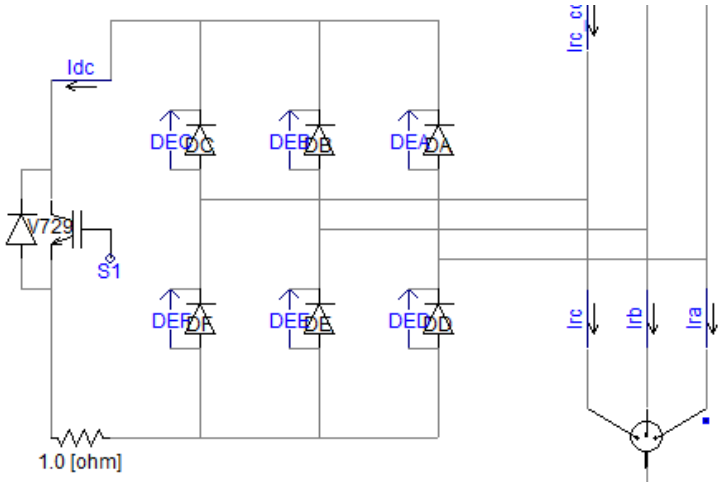

Fig. 4.20 Model for crowbar circuit

In the model, RSC protection is based on the magnitude of rotor currents fed to grid. The rotor currents are transformed to dq components and further overall the magnitude Ir is calculated. (Fig. 4.21)

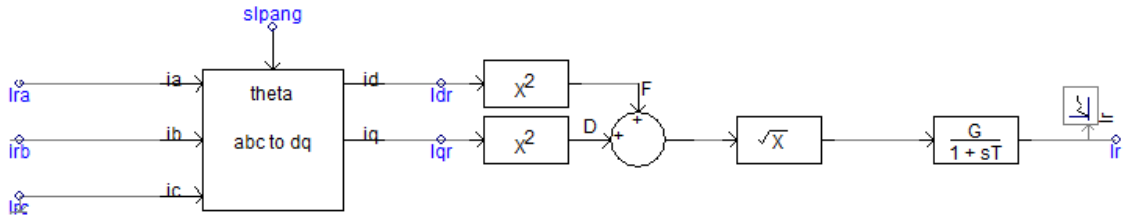

Fig. 4.21 Model for calculation of rotor current in crowbar circuit.

Then the magnitude of *Ir* is compared to the threshold value, and if the current value exceeds then the signals is originated by comparator to switch *S1* on the protection circuit. The rotor currents are bypassed to a resistive circuit as shown in circuit. (Fig. 4.22)

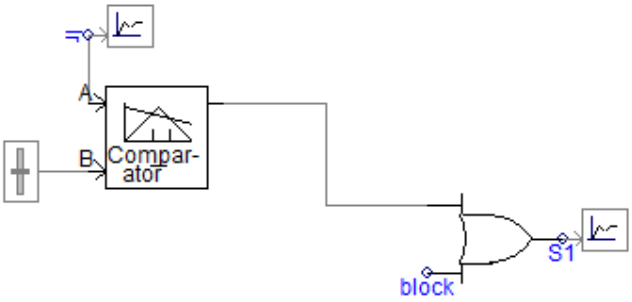

Fig. 4.22 Model for switching operation of crowbar circuit.

CHAPTER 5

RESULTS AND DISCUSSIONS

5.1 GENERAL WAVEFORMS OF WECS PERFORMANCE

The Induction machine is made to operate on speed control mode from $0 < t < 0.5$ sec. and then mode is changed to torque control mode. Until this time ($t = 0.5$ sec.), the machine will rotate at the selected rotor speed as specified $\omega = 1.054$ p.u. So the Waveforms obtained from 0.5 sec. to 3 sec. gives the response to torque control mode of induction machine. In other words it is grid interconnection response.

At $t = 3$ sec. fault occurs, for the duration of 0.15 sec. The dynamic variation of active power, reactive power, mechanical torque and rotor speed is analyzed for stability aspects. Also the induction machine is subjected to the step change in the wind speed at $t = 8$ sec. The waveform showing the variation in parameters has been observed. This would cause speed controller to react and maintain the tip speed ratio for maximum power tracking.

The induction machine is made to operate in super synchronous mode, ($\omega = 1.05$). The rotor side converter is based Current Reference PWM. It is selected in this model to control the dynamic variations in rotor speed ω and reactive power Q_g supplied to grid. Also the control scheme selected for GSC is based on VOC. This controls active and reactive power (P_g & Q_g) supplied to grid.

Now the model is run for grid connectivity, fault & change in wind speed consecutively at different time instants and the variations in supply voltage, wind speed, electromagnetic torque mechanical torque, active & reactive power are analyzed. The waveforms and relevant explanations are given below

5.1.1 Voltage waveforms

The waveform of V_s is shown (Fig. 5.1), at the time of grid connectivity, small spikes are observed. These exist for 0.2 sec. When fault occurs at $t = 3$ sec., voltage magnitude dips 0.38 p.u. from 0.7 p.u.

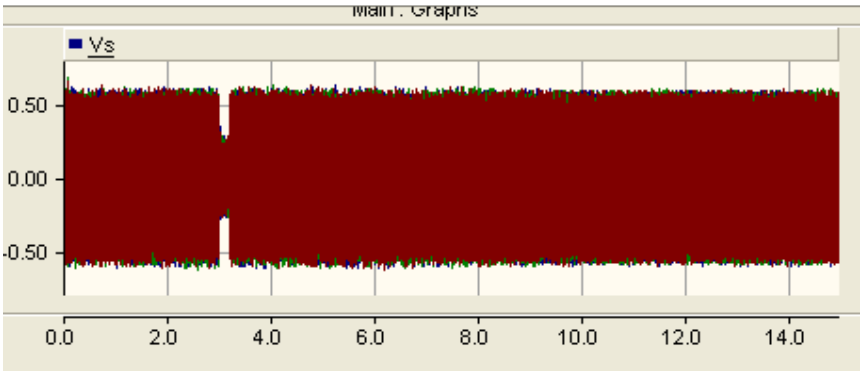

Fig. 5.1 Voltage magnitude (in p.u.)

Similarly during the fault, the rms voltage experiences the same dip that is from1.06 p.u. to 0.42 p.u. (Fig. 5.2)

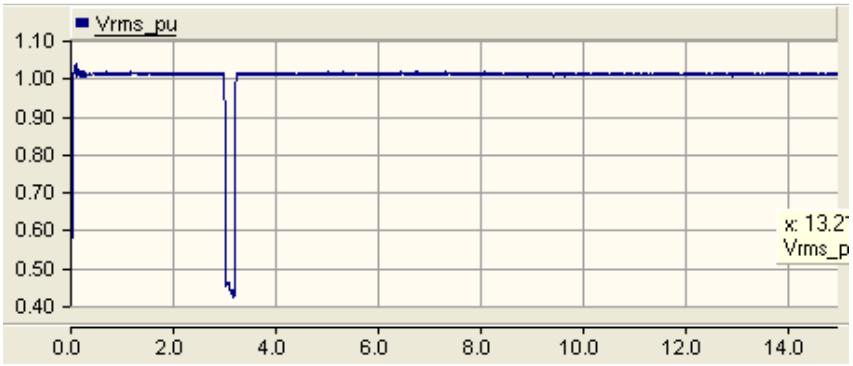

Fig. 5.2 RMS Voltage (in p.u.)

It is observed that with the occurrence of fault in the transmission line, the grid side voltage dips and with the effect of control schemes the voltage magnitude is recovered in short duration. (i.e. 0.15 sec.)

5.1.2 Rotor speed waveforms

The dynamic response of rotor speed at the grid interconnection can be observed from t = 0.5 sec. When torque control mode is enabled at 0.5 sec., the rotor speed dips up to 1.05 p.u. and further retains its reference value W_{ref} i.e. 1.055 p.u. at 2.8 sec. It stabilizes at 2.8 sec. i.e. within 1.3 sec. In case of fault, rotor speed rises and oscillates. The peak of spike reaches to 1.088 p.u. It gets stabilize at 5.8 sec. i.e. within 2.8 sec. (Fig. 5.3)

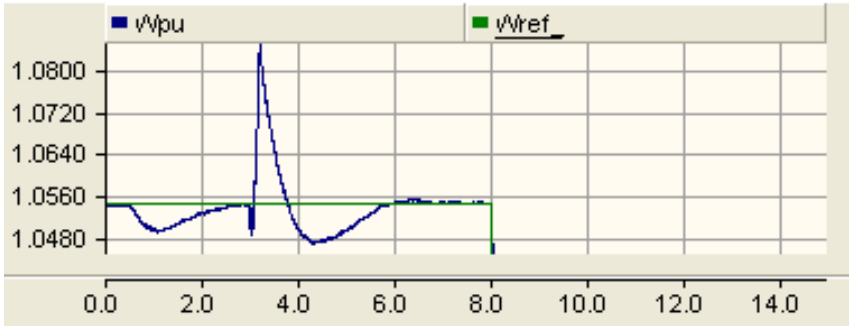

Fig. 5.3 Rotor speed (in p.u.)

The wind speed changes to 10.5 m/sec. from 11.5 m/sec. at t = 8 sec. For the response to the step change in wind speed, the rotor speed ω decreases as W_{ref} decrease. The W_{ref} reduces to 0.97 p.u. and in response ω decreases and reaches negative peak up to 0.92 p.u. the rotor speed stabilize itself and reaches reference speed 0.962 p.u. at 12.5 sec. (i.e. 4.5 sec. to achieve W_{ref}) (Fig. 5.4 & 5.5)

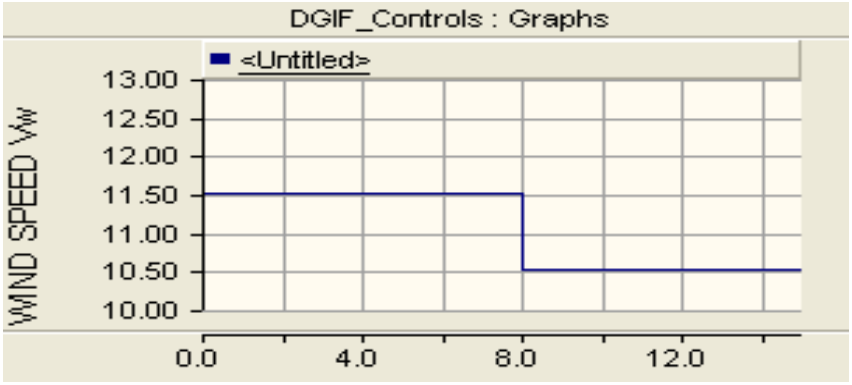

Fig. 5.4 Wind speed (m/sec.)

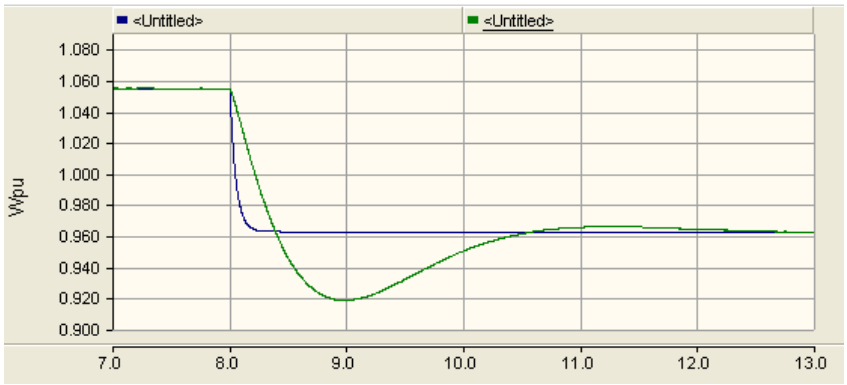

Fig. 5.5 Rotor speed (in p.u.)

Thus it can be seen that rotor speed kept its magnitude within tolerable limits, and stabilizes itself by achieving reference speed in short time. The generating system sustains the abnormal conditions.

5.1.3 Torque Waveforms

As the model is run at torque control mode, the magnitude of torque must remain constant for normal conditions and must be in limits for proper stability. From the waveforms, the electrical torque has nominal value of – 0.6 p.u. & when disturbance occurs at the time of fault. i.e. at t = 3 sec. The T_E reduces & oscillates and gets stabilize to its magnitude again, within 0.6 sec. As the wind speed decreases, active power decreases and hence decreasing torque begins to decelerate rotor speed, the decelerating torque being the difference between the turbine mechanical torque and the torque given by the optimum curve. Eventually the machine will reach where the decelerating torque is zero i.e. electromagnetic torque equals to mechanical torque, the value of T_E reduces to –0.5 p.u gradually. (Fig. 5.6)

$$T_E - T_M = J\, dW_{pu}/dt \qquad (5.1)$$

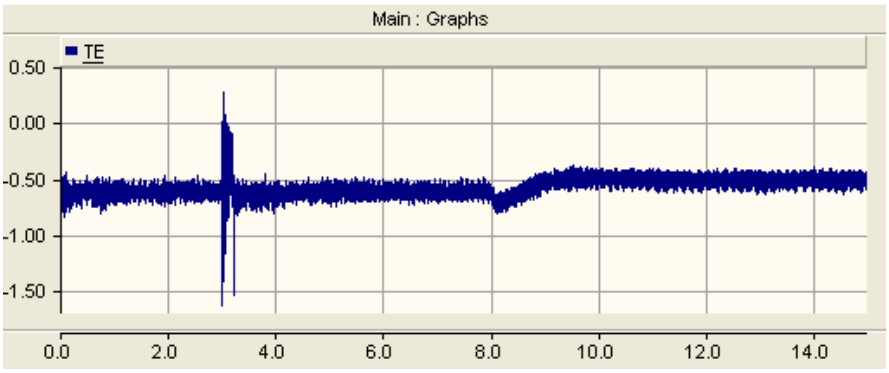

Fig. 5.6 Electromagnetic torque (in p.u.)

The mechanical torque oscillates in speed control mode and when the mode is shifted to torque control, the T_M magnitude becomes constant. According to waveform, the magnitude becomes – 0.62 p.u. In the case of fault, oscillations in T_M are observed for the duration of 0.5 sec. The oscillations reaches peak at 0 p.u. and – 1.5p.u. Further when wind speed decreases at 8 sec., magnitude of T_M rises from – 0.62 to – 0.52 p.u. (Fig. 5.7)

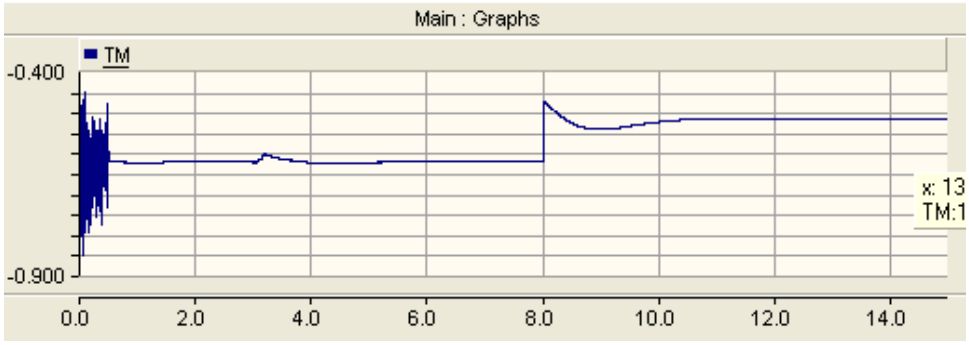

Fig. 5.7 Mechanical torque (in p.u.)

Hence it can be observed from the model, that torque magnitude approximately remains same. There is considerable variation of magnitude when subjected to wind speed variation or fault conditions and these variations are stable.

5.1.4 Voltage, Current, Active Power & Reactive Power Waveforms

The stator side voltage and current at the time of prefault & fault & postfault are shown in Fig. 5.8. Up to 3 sec. the voltage magnitude is 0.56 p.u. and for current is 0.1 p.u. At the time of fault, the peak magnitude of voltage decreases from 0.56 up to 0.23 p.u. And the stator current increases from 0.1 p.u. upto 0.56 p.u. in same region of waveform. The postfault response is similar to that of the prefault conditions. (Fig. 5.8)

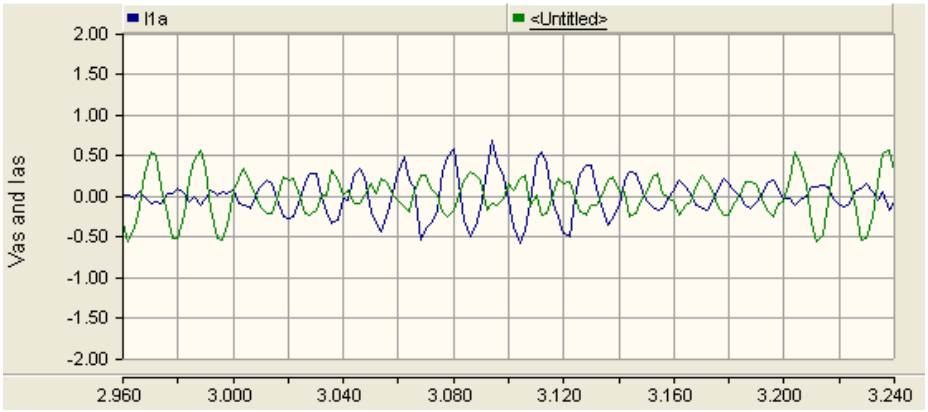

Fig. 5.8 Stator voltage & Stator current

At prefault condition, the voltage and current waveform maintains 180^{o} approximately phase angle between them. So the active power supplied is almost constant. But in fault duration, voltage dips and current spikes, hence the phase angle shifts from 180^{o}. Therefore the active power dips in fault region and the reactive power oscillations are produced.

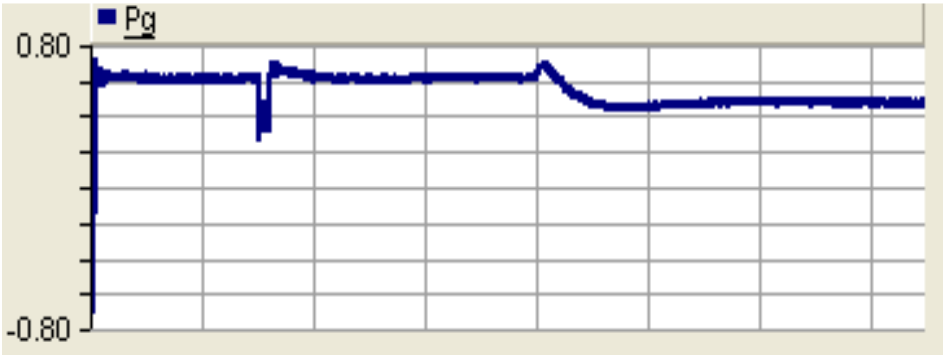

Fig. 5.9 Active power supplied to grid (in p.u.) (0 < t < 16 sec.)

The above waveform corresponds to active power fed to grid. The variation in power is due to grid interconnection, fault and step change in wind speed sequentially. In speed control mode, the spike of negative magnitude is about – 0.7 p.u. When torque control mode enables, power achieves constant value of 0.62 p.u. Further at the time of fault, (t = 3 sec.) active power dips to the value of 0.22 p.u. The power waveform stabilizes within 1 sec. from the starting of fault and retains its value of 0.62 p.u.. At last the power gets decrease due to drop in wind speed, and the magnitude shifts to 0.42 p.u. within 2 sec. (Fig. 5.9)

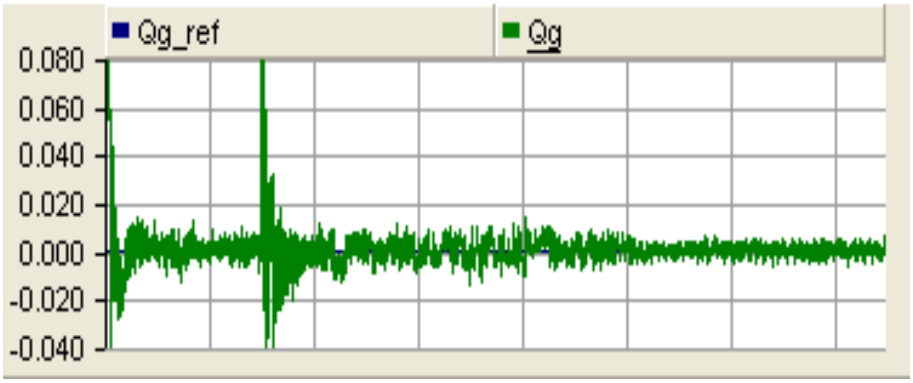

Fig. 5.10 Reactive power supplied to grid (in p.u.) (0 < t < 16 sec.)

Similarly the reactive power is supplied at the time of fault or grid interconnection in order to maintain the voltage magnitude in limits. The reactive power supply is observed as a spike (0.06 p.u.) in speed control mode (0 to 0.5 sec.) while grid interconnection.(Fig. 5.10) At the time of fault (3 to 4 sec.) the reactive power again high magnitude oscillations of about 0.8 p.u. These oscillations persist for 1 sec. approximately. This controls rotor speed variation. The reactive power is almost zero for the step change of wind speed at t = 8 sec. For normal conditions the reactive power is set to zero.

At last, the inference from the waveforms can be made that active & reactive power supply is regulated better at occurrences of abnormal conditions. Also stator side voltage and current waveforms support above statement.

5.2 ROTOR SIDE CONVERTER WAVEFORMS

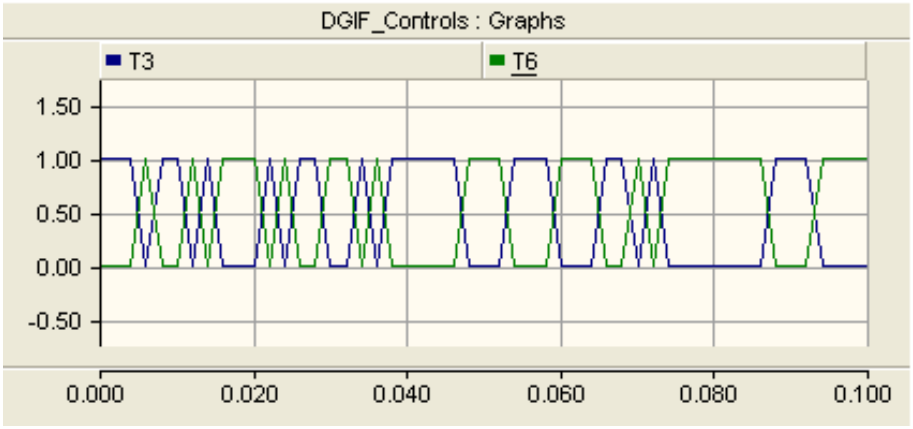

Fig. 5.11 Firing sequence of T_3 & T_6, PWM

5.2.1 Firing Pulse & Current Synthesis Waveform

The firing sequence & current waveforms refer to the grid interconnection duration. It shows more oscillations at instant of grid integration, but later it reduces. As with the explanation, the switches T_3 and T_6 are fired in consecutive in order to control the tracking of I_{rb_ref}. Switch T_3 makes the positive I_{rb} value for which the ramp function I_{rb} is generated. When I_{rb} reaches upper band value the T_6 is triggered and T_3 is turned off. Now the I_{rb} drops linearly until it reaches the lower threshold value. In this way the desired I_{rb_ref} is tracked. i.e. the I_{rb} oscillates around I_{rb_ref} . Similarly I_{ra} and I_{rc} are also synthesized. It is to control I_d and I_q component and further control reactive power and rotor speed to achieve stable system.

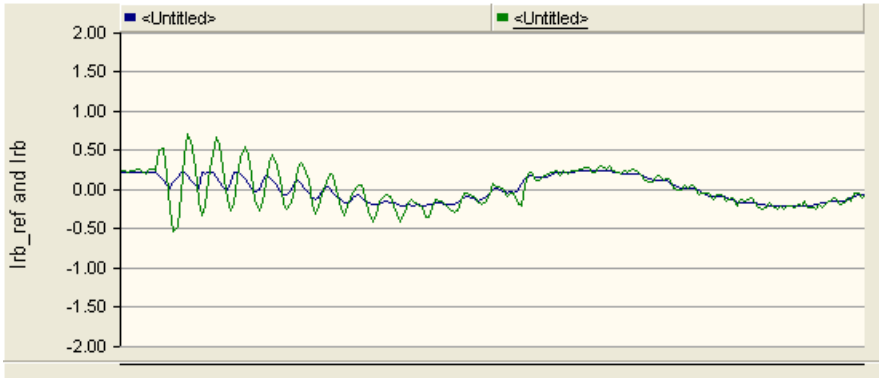

Fig. 5.12 Reference phase current waveform synthesis of phase B (0 < t < 1 sec.)

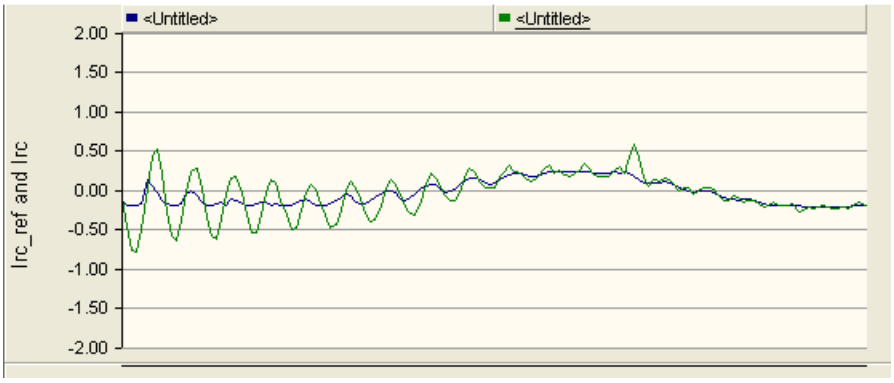

Fig. 5.13 Reference phase current waveform synthesis of phase C (0 < t < 1 sec.)

It is observed that the obtained rotor current waveforms are synthesized in better way & track reference currents. Certainly as oscillations diminishes, the waveforms makes system stable.

5.2.2 dq - axis Current Waveforms

In q axis control, the variation in reference current I_{rq} is directly related to variation in rotor speed ω. At fault, I_{rq} increases ω also increases (Fig. 5.14 & 5.3) and similar characteristics can be seen when wind speed decreases. i.e. both variables falls and takes 3 sec. approx to stabilize their magnitude (Fig. 5.14 & 5.5)

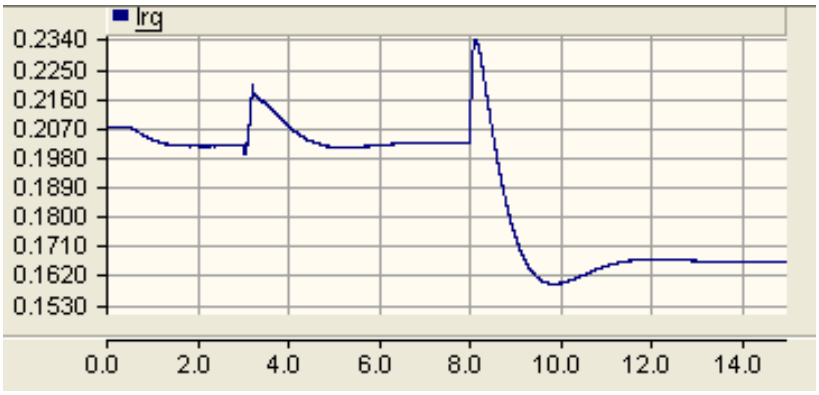

Fig. 5.14 Reference q- axis rotor current

The reactive power is controlled by the I_{rd} of the CR-PWM, the variations in I_{rd} directly proportional to Q_g. The Q_g in waveform is supplied reactive power, therefore the negative spikes in I_{rd} means positive spike in Q_g. the I_{rd} have small magnitude of about 0.071 p.u., (Fig. 5.15) this indicates that not much reactive power is supplied from the RSC in normal

conditions. Therefore Q_g oscillates around 0 p.u. because of unity power factor mode operation. (Fig. 5.10)

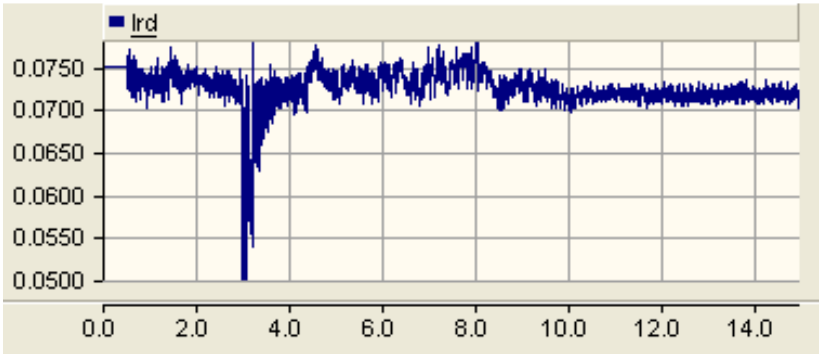

Fig. 5.15 Reference q- axis rotor current.

It is observed that the d-axis & q-axis current waveforms attain same characteristics as that of active & reactive power supply respectively. These waveforms refer to an intermediate process of control scheme implementation to converters.

5.2.3 Reference and Actual Current Waveforms

These waveforms refer to overall process of synthesis of rotor currents. As from the control scheme continuation I_{rd} and I_{rq} are transformed from by inverse *dq* transformation to 3 phase reference currents i.e. $I_{ra\text{-}ref}$, $I_{rb\text{-}ref}$ and the Fig. 5.16 of I_{ra_ref} is shown below. The current reference waveform changes its phase abruptly at abnormal conditions such as fault and wind speed reduction. Therefore the waveform seems to be distorted sinusoidal.

In later case, magnitude of current also decreases. (Fig. 5.16)

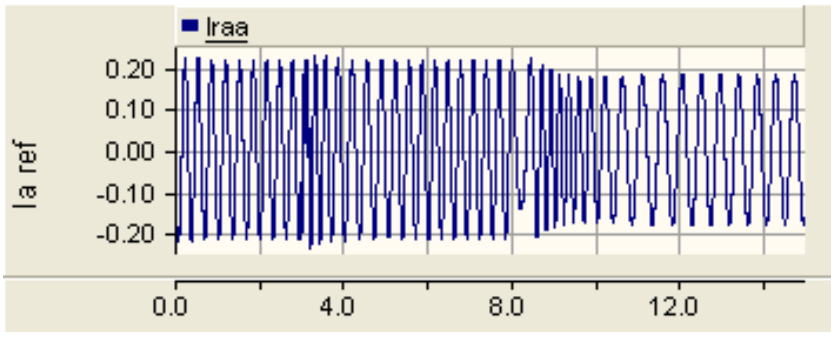

Fig. 5.16 Reference current waveform of phase a

Similarly $I_{b\text{-}ref}$ & $I_{c\text{-}ref}$ phase currents have same characteristics. In these waveforms, both actual and reference currents are incorporated

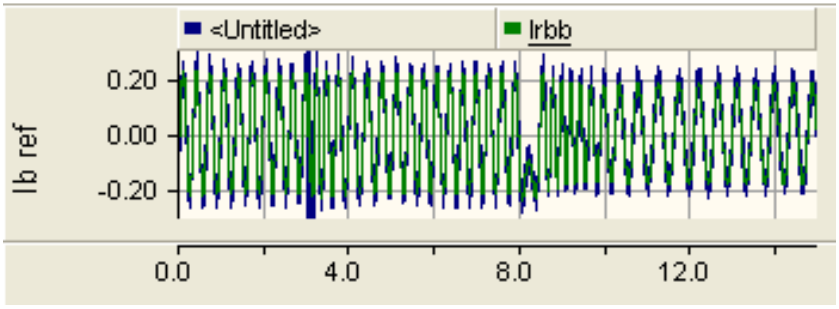

Fig. 5.17 Reference current and actual current waveform of phase b

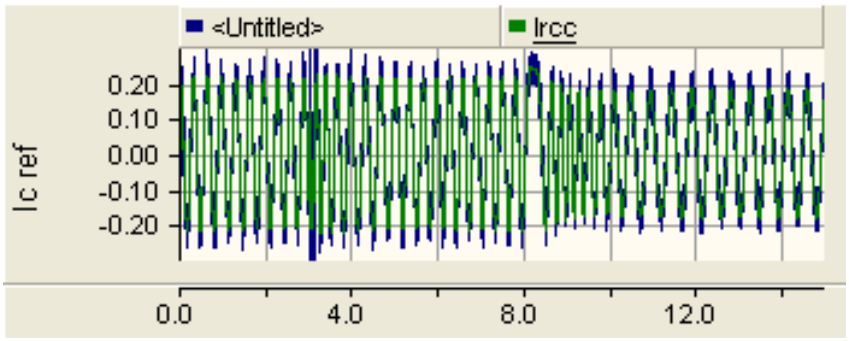

5.18 Reference current and actual current waveform of phase c

Hence the inference from the waveforms can be made that the actual rotor currents tracks the reference currents in a better way, it is observed that tracking is not smooth at fault & wind variation.

5.2.4 Slip angle Waveform

The magnitude of slip angle is used for the dq transformation; the slip angle (*slpang*) is difference between location of stator rotating flux *phis* and rotor angle *theta*. The variation of *phis* and *theta* in waveform refers to fault duration condition whereas slip angle waveform refers to whole model duration.

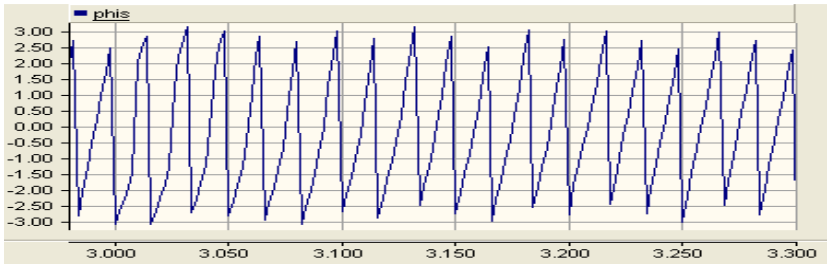

Fig. 5.19 Instantaneous location of the stator's rotating magnetic field (*phis*(ϕ_s))

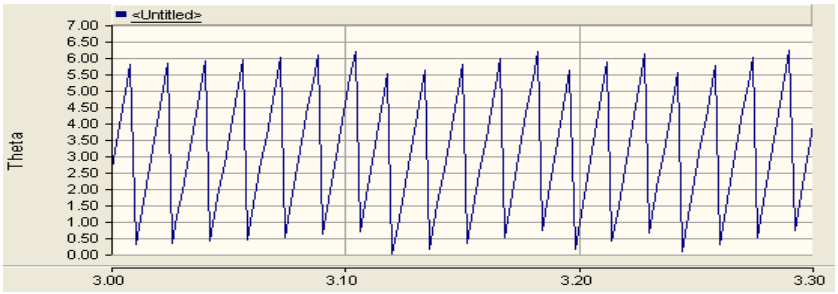

Fig. 5.20 Instantaneous location of the rotor angle *(theta(ϕ_r))*

The difference of these variables (Fig. 5.19 & 5.20) creates phase change in slip angle. (First phase distortion refers to fault and next phase distortion refers to wind speed variation in Fig. 5.21).

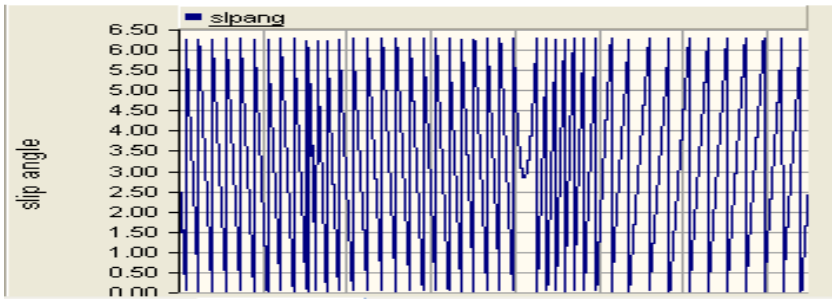

Fig. 5.21Slip angle ϕ_{slip} (3 < t < 3.3 sec.)

From the above mentioned waveforms, it is been observed that variation of slip angle is uniform in normal conditions.

5.3 GRID SIDECONVERTER WAVEFORMS

As the model is run at super synchronous mode the direction of active power will be RSC to GSC. But the dc link provides independent control to both converters.

5.3.1 DC link Voltage and d-q axis Current Waveforms

The active and reactive power supplied by RSC is based on stability criterion. While the control scheme of GSC is based on grid code requirements. The expression of power from GSC control is

$$P_g = 3/2\ [V_{dg} * i_{1d}] = E_{cap} * i_{1d} \qquad (5.2)$$

The magnitudes of capacitor voltage & stator d-axis current can be obtained from the waveforms given below. (Fig. 5.22 & Fig. 5.23)

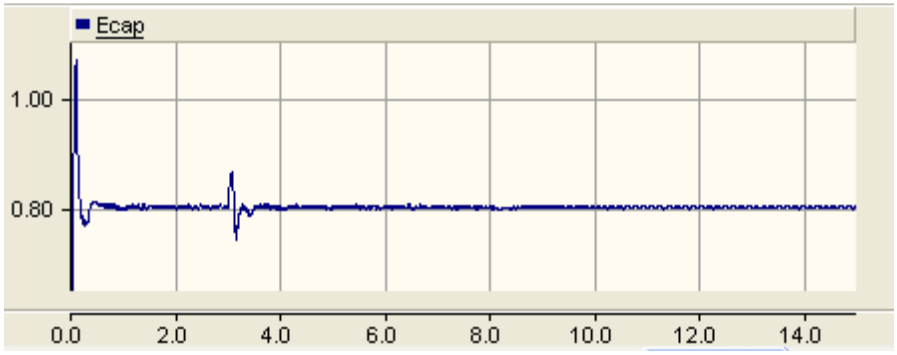

Fig. 5.22 DC link capacitor voltage (in p.u.)

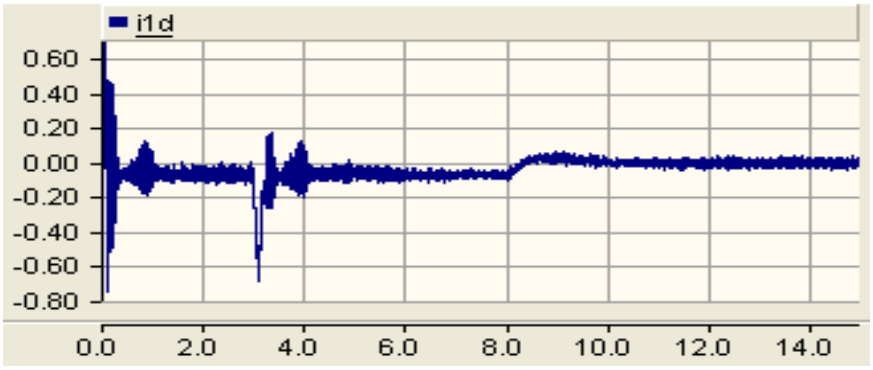

Fig. 5.23 d-axis stator current

Then the magnitude of P_g in normal conditions is

$P_g = 0.8*0.772 = 0.62$p.u. (Fig. 5.9) (5.3)

Similarly for reactive power

$Q_g = 3/2 [- V_{dg} * i_{1q}]$ (5.4)

As i_{1q} oscillates at zero in waveform (Fig. 5.24), so reactive power is just oscillating as that of $i_{1q.}$ (Fig. 5.10)

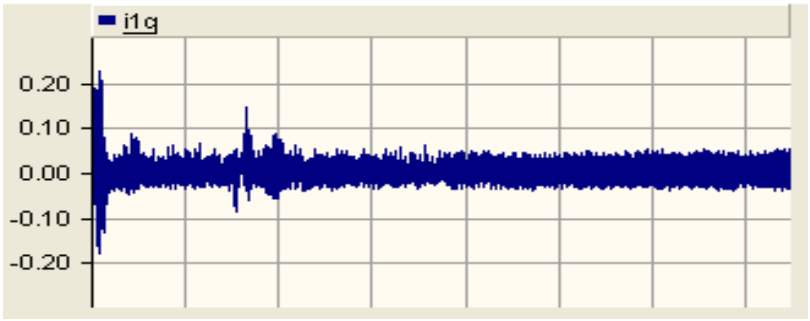

Fig. 5.24 q-axis stator current (0 < t < 16 sec.)

From the above matter, it is inferred that magnitude of active and reactive power are verified with the support of theory equation/relation.

5.3.2 d-q axis reference Voltages

The waveforms refer to the generation of reference voltages by which active & reactive power characteristics can be inferred. For the generation of reference voltage (V_{d_ref1}), d-axis reference current (I_{d_ref}) is compared to stator current (i_{1d}). (Fig. 5.25, 5.23, 5.26)

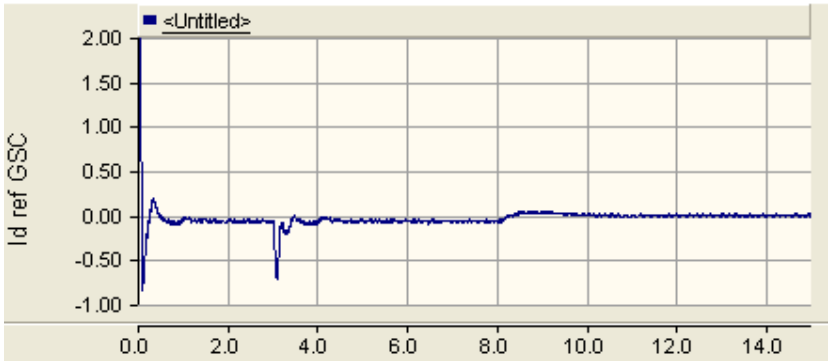

Fig. 5.25 d-axis reference current

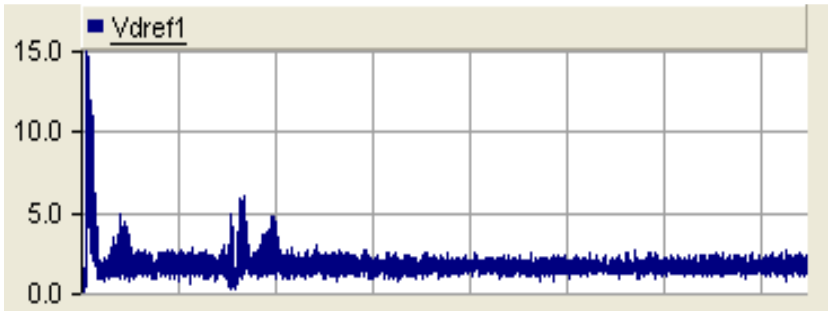

Fig. 5.26 d- axis reference voltage (0 < t < 16 sec.)

Further for the generation of reference voltage (V_{q_ref1}), q-axis reference current (I_{q_ref}) is compared to stator current (i_{1q}). (Fig. 5.27, 5.24, 5.28)

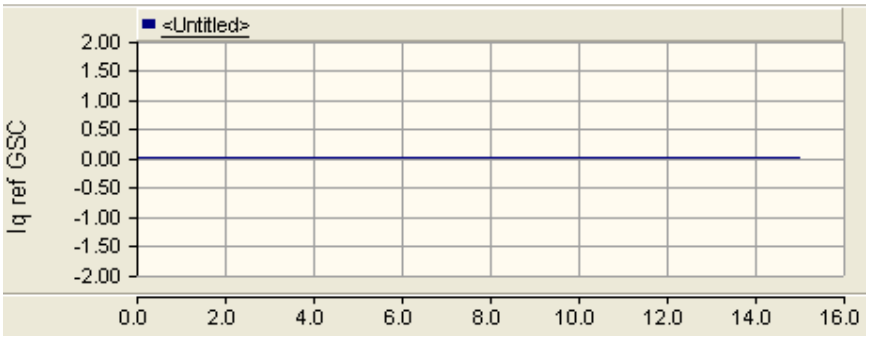

Fig. 5.27 q-axis reference current

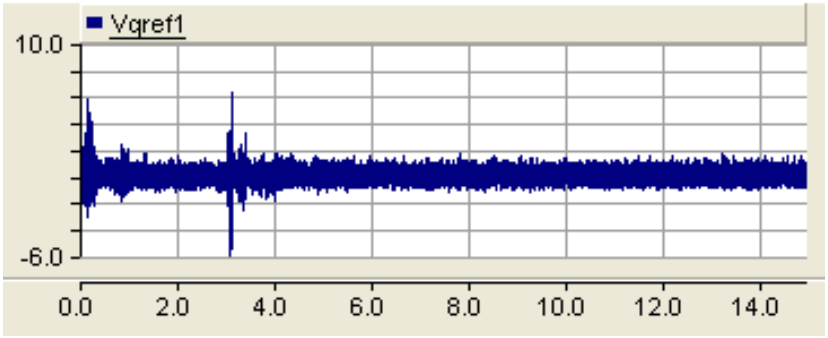

Fig. 5.28 q- axis reference voltage

It is observed that the reference voltage characteristics are similar as that of active & reactive power supply waveforms.

5.3.3 DC link voltage waveform

This waveform refers to characteristics of dc link voltage of converter system. The magnitude of voltage must remain same in normal as well as in abnormal conditions, but this can be in ideal case. From the theory, reference of magnitude of dc link voltage (i.e. E_{capref}) depends on phase voltage magnitude and modulating index. (Fig. 5.29)

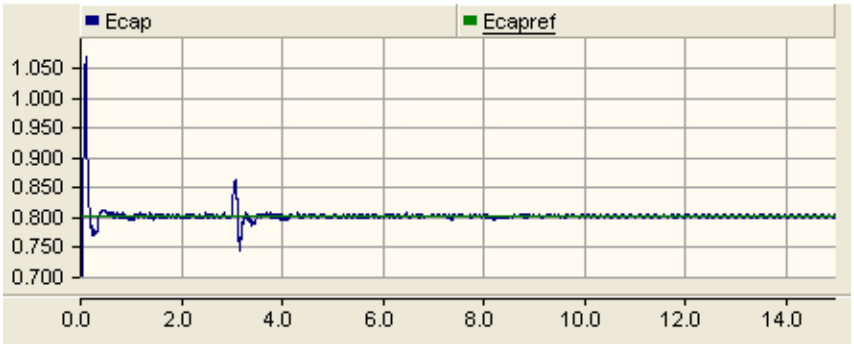

Fig. 5.29 (Reference & actual dc link capacitor voltage)

$$E_{capref}^{*} = \sqrt{6} * V_{ai1} / m_a = 2.45*0.28/0.85 = 0.80 \text{ p.u.} \quad (5.5)$$

Also (V_{ai1} = 0.69/$\sqrt{2}$ *3 = 0.28), Where V_{ai1} fundamental component of phase voltage. The E_{cap} oscillates at the time of grid connectivity and fault. In normal conditions, the value of $E_{cap} = E_{capref.}$

It is inferred that the waveform gives better characteristics as required for the simulation; the dc voltage magnitude remains constant at normal and controlled spike in abnormal conditions.

5.4 CONDITIONAL WAVEFORMS

5.4.1 Fault waveforms

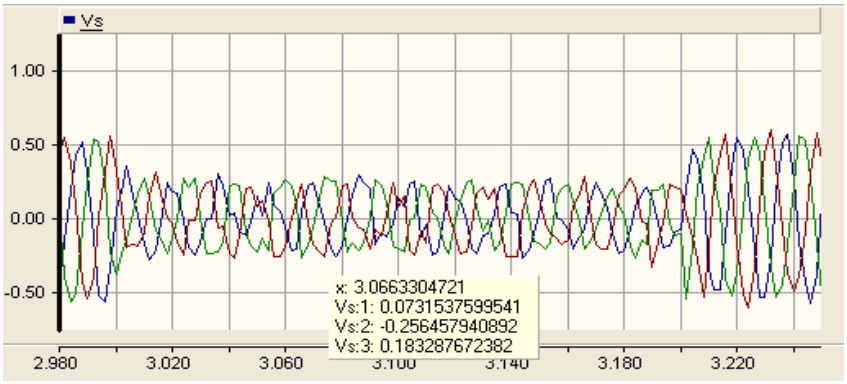

Fig. 5.30 Voltage waveform at fault (3 to 3.2 sec.)

In the fault duration, the voltage dips (Fig. 5.30) which is controlled by the supply of reactive power to the grid. The reactive power spikes at the time of fault, as from the Fig. 5.31. It reaches to 0.255 p.u. due to this the voltage is restored within 0.2 sec. i.e. at 3.2 sec. the voltage was restored.

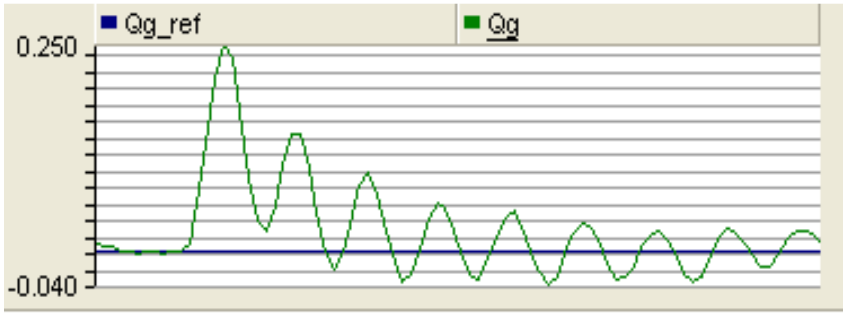

Fig. 5.31 Reactive power waveform at fault (3 to 3.2 sec.)

The reactive power is control by proper firing sequence of the GSC. The firing sequence of GSC at fault conditions is given if Fig. 5.32.

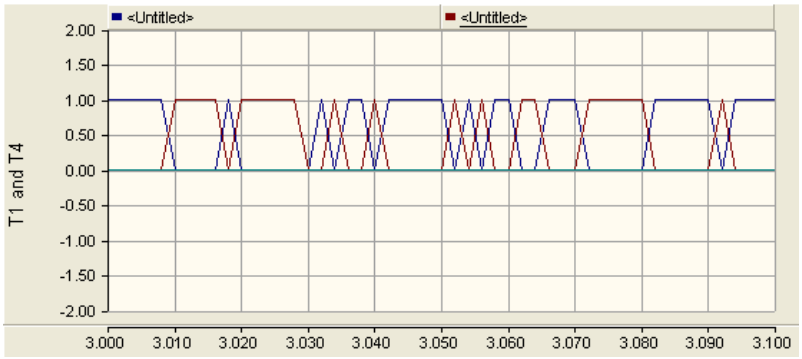

Fig.5.32 Firing sequence of GSC in fault condition

In fault condition, stator voltage decreases and stator current increases. The voltage &current of phase *a* is shown in waveforms. (Fig. 5.33 &5.34)

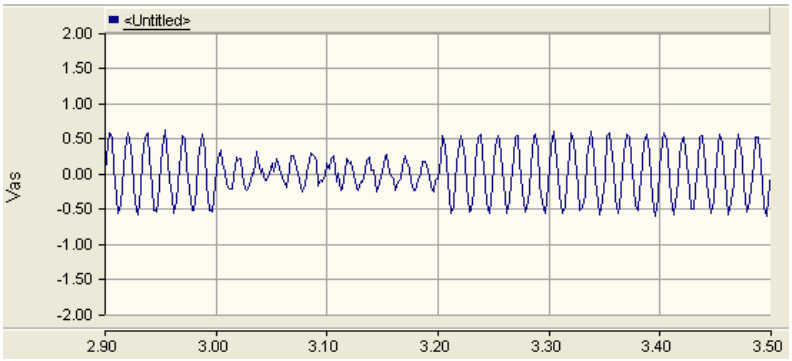

Fig. 5.33 Stator voltage of phase a

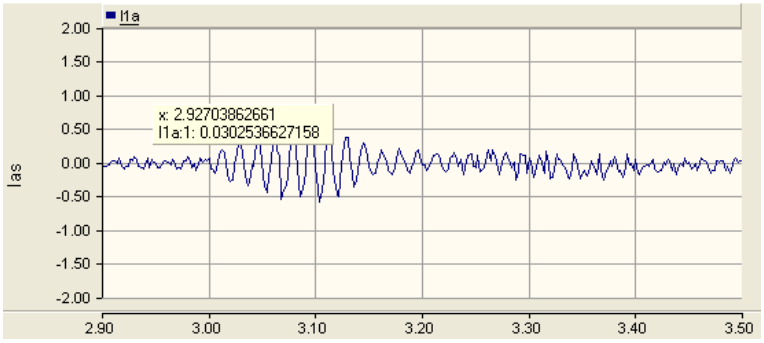

Fig. 5.34 Stator current of phase a

It is observed that all waveforms link one another for the aim to reduce the effect of fault (such as voltage dip), i.e. with proper firing sequence achieved, reactive power supply is controlled so as to compensate for the voltage dip.

5.4.2 Grid connection waveforms

During grid interconnection, the high magnitude of stator current spikes is observed (about 1.4 p.u.) and later it reduces and achieves steady state condition. (Fig. 5.35) The power factor is poor at starting and later achieves almost unity as can be seen from Fig. 5.36.

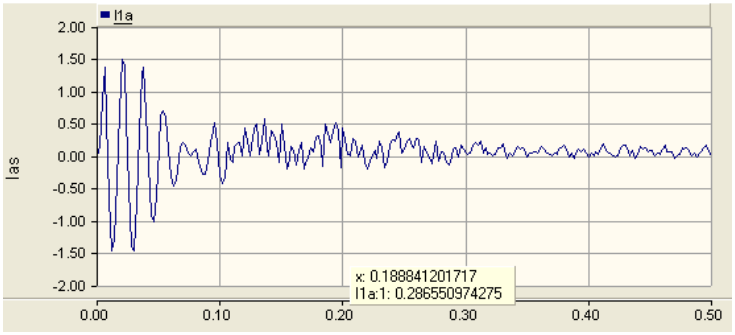

Fig. 5.35 Stator current of phase a in fault condition

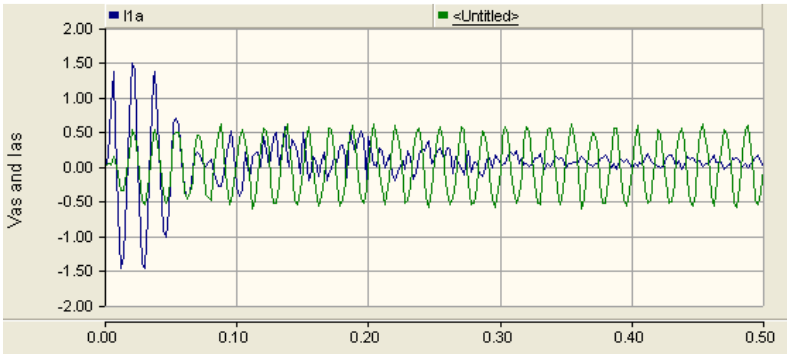

Fig. 5.36 Stator voltage & stator current of phase a in fault condition

It is observed from the waveforms that grid integration is not an instant lock up for the generating system; it takes sufficient time to integrate the new system. The waveforms produce oscillations at starting; here these are in controlled magnitude. Further oscillations are reduced and stable operation is achieved.

5.4.3 Change in wind speed Waveforms

The variation of stator rotating flux and rotor angle during the wind speed variation are shown in Fig. 5.37 & 5.38.

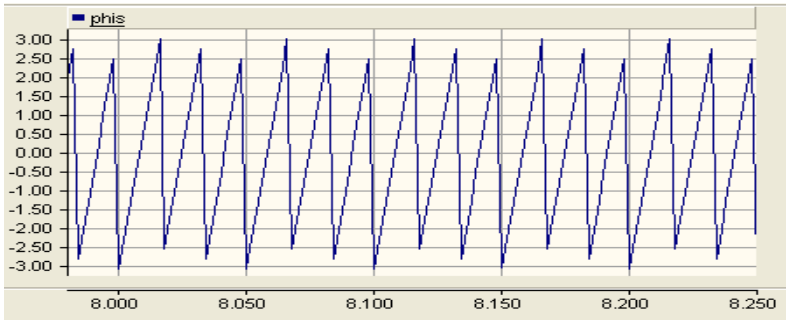

Fig. 5.37 Stator's rotating magnetic field (*phis*(ϕ_s))

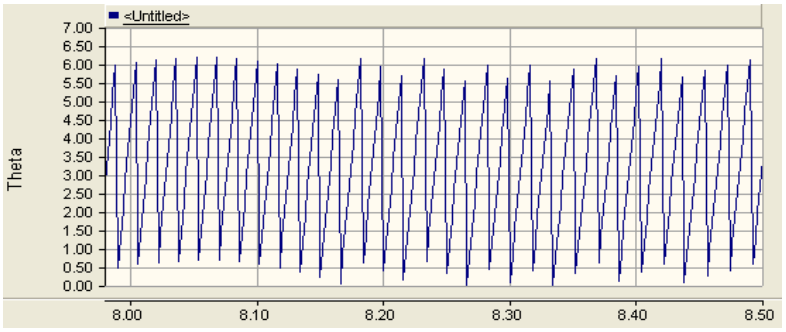

Fig. 5.38 Rotor angle *(theta*(ϕ_r))

For the determination of slip angle both of them are compared. The difference of stator rotating flux and rotor angle can be seen in Fig. 5.39.

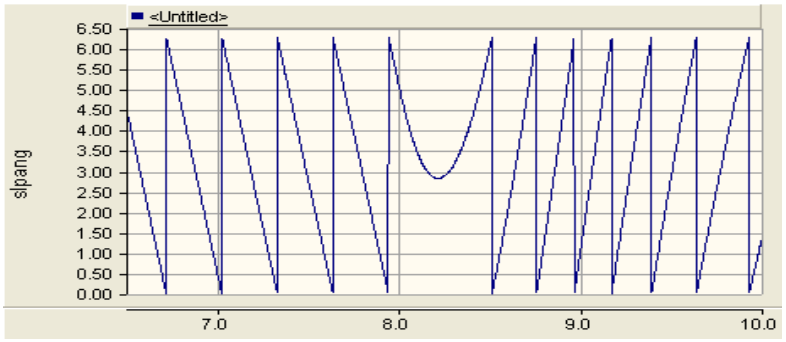

Fig. 5.39 Slip angle ϕ_{slip}

It is observed that the phase of the slip angle changes as the variation in wind occurs. This means that slip angle modifies its characteristics in accordance to new dynamics of rotor speed/ generating system. It is to provide proper *dq* transformation for smooth performance of generating system at variation of wind.

5.5 CROWBAR PROTECTION WAVEFORM

The rotor current Ir has constant magnitude of 0.22 p.u. in normal conditions, at the condition of fault, it spikes to 0.7 p.u. which is below the threshold value. So the switch S1 is at off state i.e. at 0. i.e. during fault conditions, converters are not disconnected from the circuit. (Fig. 5.40)

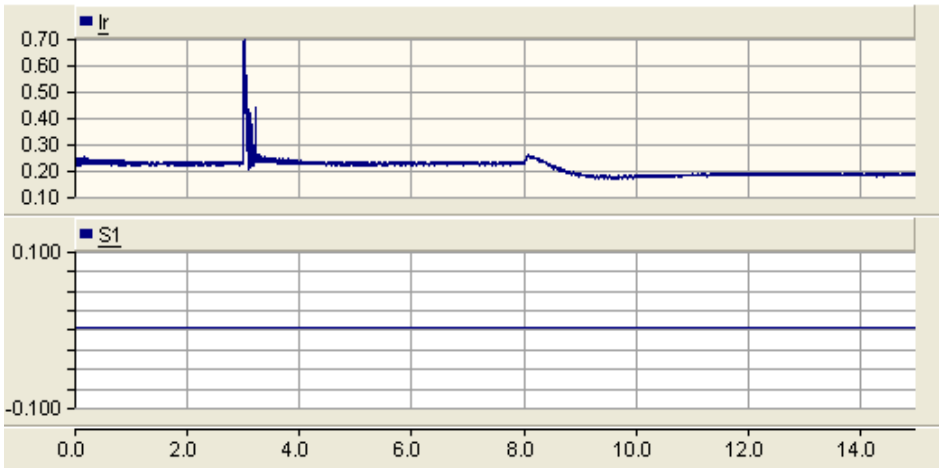

Fig. 5.40 Magnitude of rotor current & status of crowbar switch

It is observed that the crowbar protection do not switches ON for account of rotor fault current (*Ir*) spike. It means that the rotor fault current is not so much that protection system enables.

CHAPTER 6

CONCLUSION AND FUTURE SCOPE

The dynamic behaviour/response of DFIG based WECS connected to grid is investigated. Wind turbine is controlled by successfully implemented control techniques. The dynamic variation of output parameters of model, such as active & reactive power supply, electrical & mechanical torque, rotor speed, stator voltage & current etc are kept in limits and the desired magnitudes are achieved in short time by proper tuning of industrial controllers (PI Controllers), though technically it is difficult to tune SFO. These desired responses are achieved even when model is subjected to grid integration, fault and wind speed variation.

In future scope,

1. For the model, the wind turbine may be extended to wind park.
2. The stability of the SFO scheme can be increased more by using other tuning techniques.
3. The model can be modelled for unsymmetrical faults also.

REFERENCES

[1]. Wind power data [online]. Available: http://www.thewindpower.net

[2]. B.H. Chowdhury, S. Chellapilla, "Double-fed induction generator control for variable speed wind power generation," *Electric Power Systems Research*, vol-76, iss. 9-10, pp. 786-800, 2006.

[3]. L.M. Craig, M. Davidson, N. Jenkins, A.Vaudin, "Integration of wind turbines on weak rural networks," in *Proc. 1996 Opportunities Adv. Int. Power Gen.*, no. 419, pp. 419–164.

[4]. R.Allan, N. Jenkins, F.Castro, Z. Saad-Saoud, J. Roman, M. A. Rodrigues, P. Gardner, M. Birks, J. Coneybeare, and A. Ferguson, "Large wind turbines and weak rural electricity systems," *BWEA Conference*, 1994.

[5]. R. Datta and V. T. Ranganathan, "Variable-speed wind power generation using doubly fed wound rotor induction – a comparison with alternative schemes, *IEEE Trans. Energy Conversion*, vol. 17, no. 3, pp. 414-421, Sept. 2002.

[6]. W. Qiao, R. G. Harley, "Power quality and dynamic performance improvement of wind farms using a statcom," *IEEE Power Electronics Specialists Conference*, pp. 1832-1838, 2007

[7]. M.Y. Uctug, I. Eskandarzadeh, H Ince, "Modelling and output power optimization of a wind turbine driven double output induction generator", *IEE Proceeding on Electrical power Applications*, vol. 141, No. 2, 1994.

[8]. A. Larsson, "Flicker emission of wind turbines during continuous operation," *IEEE Trans. Energy Conversion*, vol. 17, no. 1. pp. 114-118, Mar. 2002.

[9]. V. Akhmatov, "Analysis of dynamic behavior of electric power systems with large amount of wind power," Ph.D. thesis, Technical University of Denmark, Kgs. Lyngby, Denmark, Apr. 2003.

[10]. G. A. Smith, K. A. Nigim,"Wind-energy recovery by a static Scherbius induction generator", *IEE Proc.* vol.*128*, pp. 317-324, 1981

[11]. S. Engelhardt, I. Erlich, C. Feltes, J. Kretschmann, F. Shewarega, "Reactive Power Capability of Wind Turbines Based on Doubly Fed Induction Generator," *IEEE Trans. on Energy Conversion*, vol. 26, no. 1, pp. 364-372, March 2011

[12]. S. Muller, M. Deicke and R.W. de Doncker, “Doubly fed induction generator systems for wind turbines,” *IEEE, Industry Applications Magazine*, vol. 8, iss. 3, pp. 26-33, May/June 2002.

[13]. M. V. A. Nunes, J. A. P. Lopes, H. H. Zurn, U. H. Bezerra, R. G. Almeida, “Influence of the variable-speed wind generators in transient stability margin of the conventional generators integrated in electrical grids,” *IEEE Trans. Energy Conversion*, vol. 19, no. 4, pp. 692-701, Dec. 2004

[14]. J. Morren and S. W. H. de Haan, “Ride through of wind turbines with doubly-fed induction generator during voltage dip,” *IEEE Trans. Energy Conversion*, vol. 20, no. 2, pp. 435-441, Jun. 2005.

[15]. L. Xu, D. Zhi, and B. Williams, “Predictive current control of doubly fed induction generators,” *IEEE Trans. Industrial. Electronics*, vol. 56, no. 10, pp. 4143–4153, Oct. 2009.

[16]. P. C. Krause, O. Wasynczuk. S. D. Sudhoff, “Analysis of electric machinery and drive system”, IEEE Press Power Engineering Series. pp l41-l87.2002

[17]. N. Mohan, T. M. Undeland, and W. P. Robbins, *Power Electronics: Converters, Applications and Design*, Clarendon Press, Oxford, UK, 1989.

[18]. S.R. Jones, K. Jones, “Control strategy for sinusoidal supply side convertors’, TEE Colloquium on *Developments in real time control for induction motor drives*, Digest 1993/024, February 1993.

[19]. W. Leonard, “Control of Electrical Drives”, Springer, New York, 2001

[20]. P.C. Krause, O. Wasynwuk, M.S Hildebrandt,”Reference frame analysis of the slip energy recovery system”, *IEEE Trans*, EC-3, (2). pp. 404-408, 1988

[21]. Z.M. Salameh, L.F.Kazda “Commutation angle analysis of a double output induction generator using a detailed *d-q* model”, *IEEE Trans*, PAS (104), (3). pp. 512-518, 1985.

[22]. R. Pena, J. C. Clare, and G. M. Asher, “Doubly fed induction generator using back-to-back PWM converters and its application to variable-speed wind-energy generation,” *IEE Proc. Elect. Power Appl.*, vol. 143, no. 3, pp. 231-241, 1996.

[23]. W.L Kling, H. Polinder, J.G. Slootweg, "Dynamic modeling of a wind turbine with doubly fed induction generator." *Power engineering Society Summer Meeting.* Vancouver, Canada. July 2001.

[24]. T.S. Jayader,”Windmills stage a comeback”, *IEEE Spectrum*, 13, pp. 45-49, 1976.

[25]. I. Cardici, M. Ermis, ”Double-output induction generator operating at subsynchronous and supersynchronous speed: steady state performance optimisation and wind-energy recovery”, *IEE proc. B,*139, (5), pp. 429-442, 1992

[26]. T. Sun, Z. Chen, F. Blaabjerg,”Voltage Recovery of Grid-connected Wind Turbines with DFIG after a Short circuit Fault” *IEEE Power Electronics Specialist Conference*, pp. 1991-1997, 2004.

[27]. T. Sun, Z. Chen, F. Blaabjerg,”Transient stability of DFIG wind turbines at an external short-circuit fault”, *Wind Energy*, 8(3) pp 345-360, 2005.

[28]. H.J. Conraths, “Rotor Control Generator System for Wind Energy Applications”, *Proc. EPE,* 2001.

[29]. P. Rodriguez, A. V. Timbus, R. Teodorescu, M. Liserre, F. Blaabjerg, “Flexible active power generation systems during grid faults,” *IEEE Trans. Ind. Electron.*, vol. 54, no. 5, pp. 2583–2592, Oct. 2005.

[30]. B. Rabelo, W. Hofmann, J. da Silva, R. de Oliveira, S. Silva, “Reactive power control design in doubly fed induction generators for wind turbines,” *IEEE Trans. Industrial Electronics*, vol. 56, no. 10, pp. 4154–4162, Oct. 2009.

[31]. S. Vazquez, J. A. Sanchez, J. M. Carrasco, J. I. Leon, E. Galvan, “A model-based direct power control for three-phase power converters,” *IEEE Trans. Ind. Electron.*, vol. 55, no. 4, pp. 1647–1657, Apr. 2008.

[32]. L. Xu, P. Cartwright, “Direct active and reactive power control of DFIG for wind energy generation,” *IEEE Trans. Energy Conversion.*, vol. 21, no. 3, pp. 750–758, Sep. 2006.

[33]. M. Malinowski, M. P. Kazmierkowski, S. Hansen, F. Blaabjerg, G. D. Marques, “Virtual-flux-based direct power control of three-phase PWM rectifiers,” *IEEE Trans. Ind. Appl.*, vol. 37, no. 4, pp. 1019–1027, Jul./Aug. 2001.

[34]. M. Malinowski, M. Jasinski, M. P. Kazmierkowski, “Simple direct power control of three-phase PWM rectifier using space-vector modulation (DPC-SVM),” *IEEE Trans. Ind. Electron.*, vol. 51, no. 4, pp. 447–454, Apr. 2004.

[35]. S. A. Larrinaga, M. A. Rodríguez, E. Oyarbide, J. R. Torrealday, “Predictive control strategy for DC/AC converters based on direct power control,” *IEEE Trans. Ind. Electron.*, vol. 54, no. 3, pp. 1261–1271, Jun. 2007.

[36]. A. Petersson, T. Thiringer, L. Harnefors, and T. Petru, “Modeling and experimental verification of grid interaction of a DFIG wind turbine,” *IEEE Trans. Energy Conversion*, vol. 20, no. 4, pp. 878–886, Dec. 2005.

[37]. J. Carrasco, L. Franquelo, J. Bialasiewicz, E. Galvan, R. Guisado, M. Prats, J. Leon, N. Moreno-Alfonso, "Power-electronic systems for the grid integration of renewable energy sources: A survey," *IEEE Trans. Industrial Electronics*, vol. 53, no. 4, pp. 1002–1016, Jun. 2006.

[38]. S. L. Andreas Petersson, T. Thiringer, "A DFIG wind-turbine ride through system influence on the energy production," *in Proc. NORDIC Wind Power Conf.*, pp. 1–7, Mar. 2004.

[39]. J. Arbi, M.B. Ghorbal, I. Slama-Belkhodja, L. Charaabi, "Direct virtual torque control for doubly fed induction generator grid connection," *IEEE Trans. Industrial Electronics*, vol. 56, no. 10, pp. 4163–4173, Oct. 2009.

[40]. S. Shao, E. Abdi, F. Barati, R. McMahon, "Stator-flux-oriented vector control for brushless doubly fed induction generator," *IEEE Trans. Industrial Electronics*, vol. 56, no. 10, pp. 4220–4228, Oct. 2009.

[41]. D.W. Zhi, L. Xu, "Direct power control of DFIG with constant switching frequency and improved transient performance," *IEEE Transactions on Energy Conversion*, vol. 22, iss. 1, pp. 110-118, Mar. 2007.

[42]. O. Anaya-Lara, P. Cartwright, J.B. Ekanayake, "Electrical Stability of Large Wind Farms—Grid Connections and Modeling", *Proc. AWEA Conference*, 2004.

[43]. L. Xu, P. Cartwright, "Direct active and reactive power control of DFIG for wind energy generation," *IEEE Transactions on Energy Conversion,* vol. 21, iss. 3, pp. 750-758, Sept. 2006.

[44]. L. Xu, Y. Wang, "Dynamic Modeling and Control of DFIG Based Wind Turbines under Unbalanced Network Conditions," *IEEE Transactions on Power Systems*, vol. 22, no. 1, Feb. 2007.

[45]. T. Brekke, N. Mohan, "Control of a doubly fed induction wind generator under unbalanced grid voltage conditions," *IEEE Transactions on Energy Conversion*, vol. 22, iss. 1, pp.129-135, Mar. 2007.

[46]. A. Petersson, "Analysis, modeling and control of doubly fed induction generators for wind turbines," Ph.D. dissertation, Chalmers Univ. of Technol., Gothenburg, Sweden, 2005.

[47]. E.Muljadi, T. Batan, D.Yildirim, C. P. Butterfield, "Understanding the unbalanced-voltage problem in wind turbine generation," in *Proc. 1999 Ind. Appl. Conf.*, vol. 2, pp. 1359–1365.

[48]. H. Akagi, H. Sato, “Control and performance of a doubly-fed induction machine intended for a flywheel energy storage system,” *IEEE Trans. Power Electron.*, vol. 17, no. 1, pp. 109–116, Jan. 2002.

[49]. M. Yamamoto, O. Motoyoshi, “Active and reactive power control for doubly-fed wound rotor induction generator,” *IEEE Trans. Power Electron.*, vol. 6, no. 4, pp. 624–629, Oct. 1991.

[50]. B. Mwinyiwiwa, Y. Zhang, B. Shen, B. T. Ooi, “Rotor Position Phase-Locked Loop for Decoupled P-Q Control of DFIG for Wind Power Generation,” *IEEE Transactions on Energy Conversion*, vol. 24, no. 3, pp. 758-765, Sept. 2009.

[51]. S. Li, T. A. Haskew, R. Challoo, M. Nemmers, "Wind Power Extraction from DFIG Wind Turbines Using Stator-Voltage and Stator-Flux Oriented Frames," *International Journal of Emerging Electric Power Systems*, vol. 12, iss. 3, Article 7, 2011.

[52]. B. Wu, Y. Lang, N. Zargari, S. Kouro, “Power Conversion and Control of Wind Energy System”, John Wiley 2011, pp 26-27, 12-13, 43-45, 20-22, 139-140, 144-148.

[53]. X . Xiong, H. Xin, "Research on Multiple Boost Converter Based on MW-Level Wind Energy Conversion System”, *in Proceedings of the Eighth International Conference on Electrical Machines and Systems (ICEMS)*, vol. 2, 1046-1049, 2005.

[54]. D. Burnham, S. Sanioso, and E. Muljadi, “Variable Rotor-Resistance Control of Wind Turbine Generators”, *in IEEE Power and Energy Society General Meeting (PES)*, 2009.

[55]. O. Anaya-lara, N. Jenkins, J. Ekanayake, P. Cartwright, M. Hughes “Wind Energy Generation Modelling and Control”, John Wiley, 2009, pp 4-7, 85.

[56]. F. Blaabjerg and Z. Chen, “Power Electronics for Modern Wind Turbines”, Morgan & Claypool Publishers, 2006

[57]. T. Akermann, “Wind Power in Power System”, Wiley, Ltd, 2005

[58]. E.Hau, “Wind Turbines: Fundamentals, Technologies, Application, Economics”, 2nd edition, Springer,2005

[59]. T. Burton, D Sharpe, N. Jenkins and E. Bossanyi, “Wind Energy Handbook”, Wiley, 2001.

[60]. J. Dai, D. Xu, B. Wu, N. R. Zargari,”A Unified DC Link Current Control Scheme for Grid Fault Ride-Through in Current Source Converter Based Wind Energy Conversion Systems”, *IEEE Transaction* pp1383-90, 2009.

[61]. J. Dai, D. Xu, B. Wu, N. R. Zargari," Unified DC-Link Current Control for Low-Voltage Ride-Through in Current-Source-Converter-Based Wind Energy Conversion Systems" *IEEE Transactions on power electronics*, vol. 26, No. 1, pp 288-297, 2011.

[62]. J.K.Patel, S.P.Gupta, S.P. Singh," Comparison of Control Techniques for rotor current control of Line-Excited Slip-ring IG for WECS", *International Conference on Computational Intelligence and Communication Networks,* pp 669-74, 2010.

[63]. E. D. Dorado, C. Carrillo, J. Cidr´as,"Control Algorithm for Coordinated Reactive Power Compensation in a Wind Park" ,*IEEE Transactions on energy conversion*, vol. 23, No. 4, pp-1064-1072, December 2008.

[64]. G. Abad, .J. Lo´pez, M. A. Rodrı´guez, L. Marroy, "Doubly Fed Induction Machine, Modeling and Control for Wind Energy Generation.", John Wiley, 2011, pp 40-43, 303-304, 481-483.

[65]. J. Wang, J. Dai, B. Wu, D. Xu, N. R. Zargari, "Megawatt Wind Energy Conversion System with Diode Rectifier and Multilevel Current Source Inverter", *IEEE Transaction*, pp-871-76, 2011.

[66]. K. H. J. Chong and R. D. Klug, "High power medium voltage drives," in *Proc. Power Conf*, Nov. 21–24, 2004, vol. 1, pp. 658–664.

[67]. R. D. Klug, N. Klaassen, "High power medium voltage drives Innovations, portfolio, trends," in *Proc. Eur. Conf. Power Electron. Appl.*, pp.10, 2005.

[68]. B. Wu, J. Pontt, J. Rodriguez, S. Bernet, S. Kouro, "Current-Source Converter and Cycloconverter Topologies for Industrial Medium-Voltage Drives", *IEEE Transactions on Industrial Electronics*, vol. 55, No.7, pp. 2786-2797, 2008.

[69]. N. Ammasaigounden, M. Subbiah, and M. Krishnamurthy, "Wind-Driven Self-Excited Pole Changing Induction Generators", *IEE Proceedings Electric Power Applications*, vol. 133, No. 5, pp. 315-321, 1986.

[70]. J. Birk, B. Andresen, "Parallel-Connected Converters for Optimizing Efficiency, Reliability and Grid Harmonics in a Wind Turbine", in *European Conference on Power Electronics and Applications (EPE),* pp. 1 -7, 2007.

[71]. D.B. Watson, J. Arrilliaga, T. Densem, "Controllable DC power supply from wind-driven self-excited induction machines", *Proc. IEE*, 1979, 126, (12), pp. 1245-1248.

[72]. D. Ehlert, H. Wrede, "Wind Turbines with Doubly-Fed Induction Generator Systems with Improved Performance due to Grid Requirements", in *IEEE Power Engineering Society General Meeting,* pp. 1-7, 2007.

[73]. Y. Guo, J. N. Jiang, C. Y. Tang, “Nonlinear Control of Wind Power Generation Systems,” *in Proc. IEEE Power Systems Conference and Exposition*, pp. 1-7, 15-18 Mar. 2009.

[74]. W Qiao, W Zhou, J.M. Aller, R.G. Harley, “Wind Speed Estimation Based Sensorless Output Maximization Control for a Wind Turbine Driving a DFIG,” *IEEE Trans. on Power Electronics*, vol. 23, no. 3, pp. 1156-1169, May 2008.

[75]. Hansen, G. Michalke, “Voltage grid support of DFIG wind turbines during grid faults," *in Proc. European Wind Energy Conference and Exhibition*, May 2007.

[76]. E. Tremblay, A. Chandra, P. Lagace, “Grid-side converter control of DFIG wind turbines to enhance power quality of distribution network," *in Proc. IEEE Power Engineering Society General Meeting*, Jun. 2006

[77]. J. Dai, J. Wang, B. Wu, D. Xu, N. R. Zargari,” Low Cost Current Source Converter Solutions for Variable Speed Wind Energy Conversion Systems” *IEEE International Electric Machines & Drives Conference (IEMDC)*, pp-825-830, 2011.

[78]. R. Wang, F. Lin, R. Hao, X. You, T. Q. Zhang,, “VSCF Doubly-fed induction generator control strategies and simulation research”, Presented at 3rd IEEE Conference on Industrial Electronics and Applications, 2008.

[79]. A. Gole, “Vector Controlled Doubly Fed Induction Generator for Wind Applications”, Department of Electrical and Computer Engineering, University of Manitoba, Canada and Nayak Corporation, Princeton, New Jersey. pp. 2.

[80]. C.D. Cho, S. R. Nam, S. H. Kang, S. J. Ahn, ”Modeling of DFIG Wind Turbines Considering Fault-ride-through Grid Code”, *The International Conference on Advanced Power System Automation and Protection*, pp- 1024-28, 2011.

APPENDIX A

Data set for the model components

Table 1: Wind turbine data set

Wind turbine nominal power	2MW
Nominal wind speed	11.5 m/sec
Wind speed operating range	10.5 – 12 m/sec
Rotor radius	40 m
Air density	1.225

Table 2: Wound rotor induction generator data set

Nominal power (in p.u.)	0.9
Operating voltage	0.69 KV
Nominal rotor speed (in p.u.)	1.054
Rotor speed range	0.9625 - 1.1
Rotor resistance & inductance (p.u.)	0.0067 & 0.11
Stator resistance & inductance (p.u.)	0.0054 & 0.1

Table 3: Grid Code data set

Operating voltage	20 KV
Operating Frequency	60 Hz

Table 4: Coupling Transformer data set

Rating (star-star)	1 MVA
Voltage ratio	20 / 0.68 KV